Droplet-based Millifluidic Technique for Encapsulation of Cinnamon Essential Oil: Optimization of the Process and Physicochemical Characterization

Atefeh Farahmand, Bahareh Emadzadeh, Behrouz Ghorani, Denis Poncelet

Droplet-based Millifluidic Technique for Encapsulation of Cinnamon Essential Oil: Optimization of the Process and Physicochemical Characterization

Atefeh Farahmand[1], Bahareh Emadzadeh*[1], Behrouz Ghorani [1]& Denis Poncelet*[2]

[1] Department of Food Nanotechnology, Research Institute of Food Science and Technology (RIFST), km 12 Mashhad-Quchan Highway, Mashhad, Iran, PO Box: 91895-157-356

[2] UMR CNRS 6144 GEPEA, Université de Nantes, F-44000 Nantes, France

*Corresponding authors email: Bahareh Emadzadeh: b.emadzadeh@rifst.ac.ir, Denis Poncelet: denis.poncelet@encapprocess.fr

Abstract

The "millifluidic" technique could be considered as a novel approach for encapsulation of bioactive compounds and has a promising perspective in the field of food engineering or pharmaceutical science. In this study, we aim to optimize the encapsulation of cinnamon essential oil (CEO) by droplet-based millifluidic technique with four responses: encapsulation efficiency (EE), loading capacity (LC), sphericity factor (SF) and size of calcium-alginate millicapsules. The effects of alginate concentration (20-30 g/L), flow rate of alginate (1-1.6 mL/min), and flow rate of CEO (0.6- 0.8 mL/min) were considered by a Box-Behnken design. The best concentration of chitosan as a coating layer on the optimized samples was selected based on the Young modulus of millicapsules. The regression models showed the significant effect ($p<0.05$) of the three variables on the characteristics of millicapsules. The optimal millicapsules with 3.58± 0.23 mm diameter and 0.96± 0.01 SF showed 98.96± 1.2% and 70.14±1.8% EE and LC, respectively. SEM images exhibited a rough external surface which changed to a rigid and smooth surface through the chitosan coating. The results of DSC and FTIR tests demonstrated the CEO entrapment in the millicapsules without any chemical interaction with the encapsulant materials. The disarray of crystallinity structure in XRD patterns revealed the successful encapsulation of CEO in the millicapsules. The non-Fickian case II in the mouth and small intestine and anomalous transport in the stomach were the main release mechanisms in the coated millicapsules. The release profile of CEO also fitted well with Ritger-Peppas model.

Keywords: Millifluidic, Cinnamon essential oil, Core-shell, Encapsulation, Kinetic release

1. Introduction

The rising demand for consumption of food products with health claims increases the efforts to produce functional foods that help to improve the health conditions, especially in elderly individuals beyond basic nutrition (K. Chen, Chen, Liang, & Xu, 2020; X. Chen, Qiu, Chen, Li, & Liang, 2020; Granato, et al., 2020; Granato, Nunes, & Barba, 2017; Piornos, Burgos-Díaz, Morales, Rubilar, & Acevedo, 2017). This kind of foods is fortified with bioactive compounds such as phytochemicals, minerals, and vitamins, etc., in the battle with a nutrient deficiency (Galanakis, 2021). During the pandemic, the bioactive compounds have also been reported to support the immune system against COVID-19 disease (Galanakis, 2020).

Plant essential oils consist of a variety of lipophilic bioactive compounds and volatile molecules such as phenol derivatives, sesquiterpene, monoterpenes, and aliphatic components. Metabolism and absorption of phenolic compounds in the gastrointestinal (GI) tract govern their biological characteristics. Only the released compounds in intestine are digested (Adorjan & Buchbauer, 2010). Cinnamon essential oil (CEO) obtained from *Cinnamomum zeylanicum* L., is widely used as a flavoring agent due to its unique organoleptic properties. It has also been proposed as a natural antioxidant and antimicrobial agent due to its phenolic compounds (Gong, Lee, Godec, Zhang, & Abbaspourrad, 2020). Nevertheless, interactions with food components, low solubility in an aqueous phase, high volatility, and negative impact on sensory properties of food products, especially at high concentrations, have faced the direct application of CEO in the food industry with some challenges (Hyldgaard, Mygind, & Meyer, 2012).

Besides their high volatility, the essential oils are easily decomposed due to sensitivity to environmental conditions. Current researches suggest the entrapment of essential oil into polymeric carriers intending to protect them against adverse environmental conditions (such as oxygen and light), to mask their unwanted intense odor and taste, or to provide a feasible way to

hold or handle the essential oil (Baldim, et al., 2020; Radünz, et al., 2019). Moreover, their encapsulation also helps to overcome their volatility, which leads to a reduction in their loss or uncontrolled release (Sangsuwan, Pongsapakworawat, Bangmo, & Sutthasupa, 2016).

Core-shell structures have been used as a delivery system to control the release mechanism and protect the bioactive compounds of essential oils from chemical reactions and degradation (Akamatsu & Yamaguchi, 2007). Protection of the core is achieved by a solid shell. As a matter of fact, the membrane acts as an obstacle between the capsule's interior and the surrounding environment (Caruso, Schüler, & Kurth, 1999). The size, structure, and morphology of core-shell capsules determine their application. Limitations in controlling the morphology, low reproducibility, and high polydispersity are disadvantages of conventional methods in core-shell production methods such as spray drying, solvent evaporation, self-assembly, and polymerization (W. Li, et al., 2018). Concerning the manufacturing process, there are different state-of-the-art approaches such as micro or millifluidic, co-extrusion, and co-axial electro-hydrodynamic atomization techniques. Besides, the methods are adjustable and convenient for a broad range of core and shell materials (Zhang, Huang, Si, & Xu, 2012).

In the droplet-based millifluidic encapsulation method, the CEO as a dispersed phase is directly extruded via a needle into the co-flowing fluid of alginate (continuous phase) to produce the oil-core droplets through a shear force between two immiscible phases (Martins, Poncelet, Marquis, Davy, & Renard, 2017). For capsule formation, the formed droplet at the tip of a glass tube is dropped into a calcium chloride cross-linking bath, the alginate engulfing the liquid core interacts with Ca^{2+} and produces a calcium-alginate shell. The data in the literatures reflect the interests regarding the encapsulation of oil using the millifluidic set-up to produce highly organized capsules with reproducibility (Pereda, Poncelet, & Renard, 2019; Ponrasu, Yang, Chou, Wu, & Cheng, 2020). Moreover, no toxic chemical is used during the capsule formation, and due to the millimeter size of the capsules, fast production could be observed. (Pendyala, Bithi,

98 Vanapalli, & Fernandes, 2019; Tamayol, et al., 2013). This is also an inexpensive and versatile
99 technique so that the optimization of the parameters involved in the formation of millicapsules
100 such as concentration and flow rates of phases could be easily adjusted (Martins, et al., 2017).

101 One of the factors with a vital role in the encapsulation of essential oil is selecting the
102 most appropriate shell material, which is determined based on the core properties and
103 encapsulation method (Purwanti, et al., 2018). Alginate is considered as one of the commonly
104 used biopolymers due to its unique properties such as gel formation in the presence of divalent
105 cations, biodegradability, non-toxicity, and biocompatibility (Kim, Chung, Shin, Yam, & Chung,
106 2008). Although low stability and leaching of the core through the pores of the alginate shell have
107 also been reported, the problem could be overcome by covering the millicapsules with a cationic
108 polymer like chitosan (Vandenberg, Drolet, Scott, & De la Noüe, 2001). Chitosan has been used
109 as an appropriate coating layer for the alginate millicapsules, so the final millicapsules have a
110 smoother surface with less permeability (S.-M. Koo, Cho, Huh, Baek, & Park, 2001). Good
111 mechanical strength and high stability under acidic and alkaline conditions have been shown for
112 chitosan-coated capsules (Liouni, Drichoutis, & Nerantzis, 2008).

113 Few studies on the millifluidic encapsulation of oil have more focused on the
114 fundamentals and the assessment of the production conditions regardless of the applications of
115 millicapsules and particularly their behavior in the GI tract. Martins, et al. (2017) produced
116 emulsion-loaded microcapsules using droplets millifluidic technique based on the inverse
117 gelation mechanism. They explained the parameters affecting the capsule size, sphericity, and
118 membrane thickness (Martins, et al., 2017). Pereda, et al. (2019) also used millifluidic/inverse
119 gelation to produce w/o emulsion filled millicapsules. They evaluated the effects of curing time
120 and calcium concentration on the oil content, and also the membrane thickness on the mechanical
121 characteristics of the millicapsules (Pereda, et al., 2019). In our previous study, we applied
122 millifluidic/direct gelation technique to develop oil-loaded millicapsules, and optimized the

instrumental, geometrical, and the feed solution properties of the millifluidic device (Farahmand, Emadzadeh, Ghorani, & Poncelet, 2021).

Millifluidic device as a new platform for the encapsulation of the essential oils such as CEO paves the way for the production of millicapsules with highly controlled dimensions and suitable loading capacity. Accordingly, in this study, a double-layered core-shell millicapsules with core of CEO was developed by means of a millifluidic device. A Box-Behnken design was applied to optimize the effects of process parameters (alginate concentration and flow rates of CEO and alginate) on the encapsulation efficiency (EE), loading capacity (LC), size, and sphericity of the produced millicapsules. The success of the encapsulation and some physicochemical characteristics of the chitosan-coated optimal millicapsules were investigated in terms of dimension, morphology, mechanical stability, FTIR spectroscopy, thermal and crystallinity properties. In addition, the kinetics and mechanism of the CEO release from the millicapsules in simulated conditions of GI tract were modeled.

2. Material and methods

2.1. Materials

Sodium alginate (with a molar mass of 1.57×10^5 g/mol, low viscosity, and mannuronic (M) to guluronic (G) acid ratio of 1.37), calcium chloride dihydrate ($CaCl_2.\ 2H_2O$), and chitosan powders (MW= 50-190 kDa, Degree of deacetylation: 75-85%) were purchased from Sigma-Aldrich (St. Louis, Mo, USA). Tween-20 (HLB=16.7), glacial acetic acid (CH_3COOH) (99.8%), tri-sodium citrate ($Na_3C_6H_5O_7$) with mass fraction purity>0.99, and n-hexane were supplied by Merck chemicals Co (Darmstadt, Germany). CEO was obtained from Tabib-daroo Co (Kashan,

145 Iran). All the other chemicals applied in this research were of reagent grade without further
146 purification.

147

148 **2.2. Characterization of CEO**

149 An Agilent 7890B gas chromatography connected with a mass detector (Model 5977A,
150 USA) was used to characterize the aromatic compounds of the CEO. The CEO was diluted by a
151 solvent (acetone) and subsequently injected into the device. In order to prevent damage to the
152 device filament, a 4.5 min delay-time was considered for the evaporation of the solvent/ residual
153 solvent in the sample. The gas chromatography was equipped with a HP-5MS capillary column
154 (phenylmethyl siloxane, 30 m× 0.25 mm, film thickness 0.25µm, Agilent). The injector
155 temperature was 270 ℃, and the oven temperature was programmed from 60 ℃ to 230 ˚C at a
156 rate of 5 ℃/min. The carrier gas was helium at a linear flow rate of 1 mL/min, and the injection
157 volume was 1 µL. The electron impact ionization was performed at 70 eV. Recognition of the
158 essential oil compounds was achieved by matching their mass spectra with those from GC-MS
159 libraries (Purwanti, et al., 2018).

160

161 **2.3. Preparation of alginate, chitosan, and calcium solutions**

162 Shell solution was prepared by dissolving suitable amounts of sodium alginate powder
163 (20, 25, and 30 g/L) and Tween-20 (0.6 g/L) in deionized water with a constant stirring (24h) for
164 full hydration. Tween reduces the surface tension of alginate droplet as it exits the millifluidic
165 tube. Surface tension is known as a holding force exerted on the droplet (Farahmand, et al.,
166 2021). There was no round-shaped millicapsule at the lower concentration of alginate (below 20
167 g/L), and pumping problems occurred at higher concentrations (more than 30 g/L) due to higher

viscosity. The cross-linking collector solution was obtained by dissolving an appropriate amount of $CaCl_2$ (30 g/L) in deionized water. This concentration level was selected based on preliminary tests. Chitosan as a coating solution was also prepared by dissolving required amounts of powder (2.5-15 g/L in 0.1 M acetic acid) to pH= 5.5 and kept stirred on a magnetic stirrer for 1 h (Murata, Maeda, Miyamoto, & Kawashima, 1993).

2.4. Encapsulation by double-stage millifluidic method

The core-shell millicapsules were formed using a millifluidic method with the geometry of co-axial flow focusing (**Fig.1**). The flow rates of dispersed (CEO) and continuous phase (alginate) were adjusted by two syringe pumps (New Era pump systems, Inc, NE-300, USA). The CEO was pumped using a Teflon tube (interior diameter (ID) 0.6 mm and outside diameter (OD) 1.5 mm) at rates (Q_{CEO}) of 0.6- 0.8 mL/min. The alginate solution mixed with Tween-20 (0.6 g/L) was also pumped into a Teflon tube (ID= 0.9 mm and OD= 2 mm) at rates (Q_{Alg}) of 1-1.6 mL/min. There are two possible flow regimes in the millifluidic method including dripping and getting, which can characterize the dynamics of droplet formation (Farahmand, et al., 2021). The flow rates were chosen according to the formation of dripping region in the glass tube. In this regime, the spherical droplets are formed in the millifluidic tube immediately after the two phases meet (**Fig. 1**). Both phases were co-flowed into a glass tube ID= 3.2 mm, OD= 5 mm, and length= 20 cm). By shear forces exerted between the two phases, the CEO was extruded in the alginate solution, and oil-core droplets were formed inside the glass tube (Martins, et al., 2017). The core-shell droplets pinched-off from the tip of the glass tube due to the rival forces, and they were collected in a calcium chloride collector stirred at 50 rpm at room temperature. After 30 min gelation time, the millicapsules were rinsed with deionized water, suspended in

chitosan solution for 15 min. The chitosan-coated millicapsules were kept in Ca^{2+} solutions (15 g/L) and stored at 4 °C until use.

Insert figure.1 about here

2.5. Experimental design

The impacts of the most important parameters of millifluidic system: alginate concentration (X_1: 20-30 g/L), the flow rate of alginate (X_2: 1-1.6 mL/min), and the flow rate of oil (X_3: 0.6-0.8 mL/min) as independent variables on the EE (Y_1), LC (Y_2), size (Y_3), and SF (Y_4) of the millicapsules were assessed using response surface methodology (RSM). The experiments were planned using Box-Behnken design with 17 experimental runs and 5 central points (**Table 1**). To elucidate the effect of encapsulation conditions on the responses, a second-order polynomial equation was utilized (**Eq. 1**):

$$Y=\beta_0 + \sum_{i=1}^{n} \beta_i X_i + \sum_{i=1}^{n-1} \sum_{j=i+1}^{n} \beta_{ij} X_i X_j + \sum_{i=1}^{n} \beta_{ii} X_i^2 \quad \textbf{(1)}$$

Where Y represents the measured responses, β_0 is the constant coefficient, β_i is the linear coefficient, β_j is the interaction coefficient among variables, β_{ii} is the quadratic coefficient, and X is the studied variable. Evaluation of the most suitable model was assessed using various statistical criteria. A coefficient of determination (R^2) close to 1, a covariance lower than 10, and an adequate precision higher than 4 were considered for selecting the desired model. The lack of fit test was used to check the adequacy of the fitted model. A non-significant lack of fit confirms well-fitting of the model.

Insert table.1 about here

2.6. Characterization of millicapsules

215 **2.6.1. Dimension and sphericity factor**

216 After the gelation procedure, the shape and size of the millicapsules were calculated
217 through Image J software (National Institutes of Health, USA). At least 20 millicapsules were
218 captured using a digital microscope (Dino-lite Pro, Taiwan) in each experimental run. The
219 photographs of samples were captured with 1280×1024 resolutions. 30× magnifications were
220 used for all experimental runs. The diameter of each millicapsules was calculated assuming it is
221 a circular shape. The Sphericity factor (SF) was measured as explained by (Davarcı, Turan,
222 Ozcelik, & Poncelet, 2017) (**Eq.2**):

223 $$SF= (2\ d_{min})/ (d_{max}+d_{min}) \qquad (2)$$

224 Where d is the millicapsule diameter. The SF> 0.95 was considered as spherical millicapsule and
225 0.9 <SF< 0.95 indicates oval and pear millicapsule. Lower values denoted shape deformation.

226

227 **2.6.2. Morphology**

228 The surface morphology of the uncoated and coated millicapsule was captured under a
229 field emission scanning electron microscope (FESEM) (MIRA3, TESCAN, Czech Republic) at
230 room temperature and acceleration voltage of 15 kV. Coating of the CEO-loaded millicapsules
231 with gold was performed by sputter coater for 150s at 20 mA. SEM images with different
232 magnifications from a range of 80-500 were taken at room temperature.

233

234 **2.6.3. Encapsulation efficiency (EE) and loading capacity (LC)**

235 Quantification of loaded CEO in millicapsule was achieved according to Parris, Cooke,
236 and Hicks (2005) with some modifications. 0.5 g of the oil-loaded millicapsule was dispersed in

5 mL of sodium citrate (0.055 M) (as a chelating agent for calcium ions) to de-crosslink the millicapsules. Then 5 mL n-hexane was added and the mixture was centrifuged at 5000 rpm for 5 min. The supernatant was gathered, and the absorbance of the extracted CEO was measured using a UV-Vis spectrophotometer (DR 5000, HACH) at a wavelength of 280 nm. The absorbance results of the extracted CEO were compared to the standard calibration curve of Cinnamaldehyde standard solutions (R^2= 0.99). The EE and LC of CEO were determined using to **Eq.** (**3**) and (**4**), respectively:

$$EE\ (\%) = (\text{amount of loaded CEO/ initial amount of CEO}) \times 100 \quad \textbf{(3)}$$

$$LC\ (\%) = \text{amount of loaded CEO/ weight of collected millicapsules} \times 100 \quad \textbf{(4)}$$

2.6.4. Mechanical strength

A texture analyzer (TA.XT-Plus, Stable Micro Systems, UK) equipped with a 20 mm cylindrical probe was used to measure the millicapsule's strength. A compression test was applied to assess the millicapsule deformation up to a distance of 2 mm, with a linear compression speed of 0.6 mm/min, pre-test speed of 1 mm/min, and a post-test speed of 2 mm/min. The normal force and the distance were calculated simultaneously at the upper plate (Fery & Weinkamer, 2007; Pereda, et al., 2019). The optimal millicapsules were coated using the chitosan solution (0, 0.25, 0.5, 1, 1.5% w/v prepared in 0.1 M acetic acid), and their strengths also were compared to the uncoated millicapsule. The maximum mechanical strength was the criterion to select the best concentration of chitosan solution for further studies. Each concentration of the chitosan was tested by five replications. All the experiments were measured at ambient temperature. Young modulus E (Pa), was estimated using to **Eq. 5**:

$$E = (3(1-\upsilon^2).\ F)/\ \sqrt{d.H^3} \quad (5)$$

Where F is the measured force to the millicapsule (N), d denotes millicapsule diameter (m), H is the displacement (m), and υ is the Poisson's ratio for which a value of 1/3 was assumed for the alginate millicapsule (Chan, et al., 2011).

2.6.5. FTIR spectroscopy

FTIR spectra for pure sodium alginate, CEO, chitosan powder, unloaded millicapsule, CEO- loaded millicapsule, and coated millicapsules (loaded or unloaded with CEO) were plotted from wavenumber 400-4000 cm^{-1} by a spectrophotometer (Bruker Alpha FTIR, US). Samples were prepared by grinding the millicapsule with KBr and pressed into a disk. A few CEO droplets were also placed on the KBr pellet (Hosseini, Zandi, Rezaei, & Farahmandghavi, 2013).

2.6.6. Thermal properties of millicapsule

Thermal transition characteristics of the CEO, sodium alginate and chitosan powders, unloaded, CEO-loaded millicapsules, and coated millicapsules were measured by a differential scanning calorimeter (DSC, Mettler, Toledo, Switzerland). Sample powder (about 15 mg) was sealed in an aluminum pan. DSC curve was recorded from 25 to 400 °C at a heating flux of 10 °C/min under 30 mL/min nitrogen flow (J. Li, Kim, Chen, & Park, 2016).

2.6.7. XRD

The structural changes were recorded by X-ray diffraction (XRD) (Siemens, D5000) over a 2θ range of 5-50 ° with a step angle of 0.04 °/min (Hosseini, et al., 2013). The results obtained were then used to plot the graphs using Origin 2019b (Origin lab Inc., USA) software.

2.6.8. In vitro digestion and release kinetics

The in vitro essential oil release was investigated in three phases of mouth, stomach and intestinal tract. Digestion protocols for simulated saliva fluid (SSF), simulated gastric fluid (SGF), and simulated intestinal fluid (SIF) were prepared as follows:

2.6.8.1. Simulated oral digestion

Specific ratios of salts and α-Amylase concentration in SSF was prepared according to (Minekus, et al., 2014). For the analysis, ~25 g of millicapsules were suspended in 20 mL prewarmed SSF, which the pH was adjusted (Metrohm, pH meter model 780) to 6.8 by standard solutions of 1 M (NaOH/HCl). The samples were placed in an incubator shaker (Memmert, Germany) at 37˚C and 95 rpm for 2 min (Bastos, de Sá Costa, Siqueira, & Garcia-Rojas, 2020). Interval time of sampling was 20 second.

2.6.8.2. Simulated gastric digestion

500 mL SGF was prepared by mixing 2g/100g NaCl and 3600 U/mL pepsin enzyme and pH adjusted to 2.5 with 1 mmol/L HCl. 25 grams of millicapsules treated in the oral phase were added to 500 mL of prewarmed (37˚C) SGF and was incubated for 2 h continuously shaking at

100 rpm. Sampling was performed at specific interval times (2, 15, 30, 45, 60, 75, 90, 105 and 120 min) (Gorbunova, Evteev, Evdokimov, & BANNIKOVA, 2016).

2.6.8.3. Simulated intestinal digestion

After gastric digestion, treated millicapsules were added to 400 mL SIF and they were incubated at 37˚C for 2 h at 100 rpm. SIF contained 0.7g/100g monobasic potassium phosphate, 0.1g/100g bile salts and 0.4g/100g pancreatin. The SIF solution pH was set to 7 utilizing 0.5 mmol/L NaOH. 20 min interval times were applied (Gorbunova, et al., 2016).

The mechanisms of release process were evaluated by various mathematical models such as Higuchi (**Eq. 6**), Ritger-Peppas (**Eq. 7**), Korsmeyer-Peppas (**Eq. 8**), and Kopcha (**Eq. 9**):

$$M_t/M_\infty = kt^{1/2} \qquad \textbf{Eq. 6} \quad \text{(Higuchi, 1963)}$$

$$M_t/M_\infty = kt^n \qquad \textbf{Eq. 7} \quad \text{(Ritger \& Peppas, 1987)}$$

$$M_t/M_\infty = (k.t^n)/100 \qquad \textbf{Eq. 8} \quad \text{(Korsmeyer, Gurny, Doelker, Buri, \& Peppas, 1983)}$$

$$M_t/M_\infty = A\times t^{1/2} + B\times t \qquad \textbf{Eq. 9} \quad \text{(Kopcha, Tojo, \& Lordi, 1990)}$$

In these models, M_t, M_∞, k, and t represent the value of released CEO at time t, the released CEO at infinite time, release constant, and time of release in simulated media, respectively. Furthermore, the n value in Ritger-Peppas and Korsmeyer-Peppas equations corresponds the release mechanism (for spherical capsule, $n \leq 0.43$ Fickian diffusion, $0.43 < n < 0.85$ non-Fickian diffusion (Anomalous transport), n= 0.85 case II transport, and above 0.85 shows a super case II mechanism. The A value in Kopcha model indicates the Fickian constant, but B value represents the erosion constants.

2.7. Statistical analysis

The model analysis in response surface methodology was performed by Design expert software version 10 (Stat-Ease Inc., Minneapolis, USA). Data obtained in the mechanical stability of optimal millicapsules were investigated by analysis of variance (ANOVA) and compared by Duncan test using Minitab software (version 16, Statsoft, USA).

3. Results and discussions

3.1. Identification of CEO constituents

Analysis of GC-MS chromatogram of CEO identified 10 compounds representing 99.97% (**Table 2**). CEO spectrum consisted of one major peak indicating trans-Cinnamaldehyde (84.04%). Hu, Zhang, Xiao, and Wang (2018) also reported that the major compound in the CEO spectrum was Cinnamaldehyde (64.94%) and this essential oil consisted of 89.78% aromatic compounds. Fadel, Hassan, Ibraheim, Abd El Mageed, and Saad (2019) reported that the major identified constituent of cinnamon bark oil spectrum was Cinnamaldehyde (90.2%), followed by eugenol (2.20%), and β-Caryophyllen (2.18%). The Different values of Cinnamaldehyde being reported in the previous researches might be due to the use of various extraction methods. In this study, the concentration of (E)-Cinnamaldehyde was used as a marker to measure the encapsulated CEO.

Insert table.2 about here

3.2. Millifluidic encapsulation process

3.2.1. Effect of independent variables on EE and LC

348

349 In this experimental design, the effects of independent variables on the responses were
350 analyzed using ANOVA (see **supplementary**, **Tables 1& 2**). The ANOVA for predicted models
351 showed a statistical dependency ($p<0.05$) on the variables. The fitted equations for each response
352 are reported in **Table 3**.

353

354 **Insert table.3 about here**

355

356

357 The EE values varied from 97.34 to 99.40% (**Fig. 2, A-C**). These values were
358 significantly higher than the results obtained by other CEO encapsulation methods (Muhammad,
359 et al., 2020; Noghabi & Molaveisi, 2020; Paris, Ramirez-Corona, Palou, & López-Malo, 2020).
360 Oil contents of millicapsules were in the range of 45.11-70.16% (**Fig. 2, D-F**).

361 **Fig. 2** exhibits the three-dimensional response surface plots of EE and LC as a function
362 of independent variables at different levels. A higher EE could be obtained by augmenting the
363 alginate concentration ([Alg]: 20 to 30 g/L) as a continuous phase (**Fig. 2, A**). Increasing the
364 alginate concentration and consequently, its viscosity inside the tube could forms capsules with
365 more efficiency and a stiffer shell (Gholamian, Nourani, & Bakhshi, 2020; Phawaphuthanon,
366 Behnam, Koo, Pan, & Chung, 2014). The EE of the oil is highly dependent on the cross-linking
367 degree of the alginate shell. Higher concentrations of alginate would result in a thick and dense
368 shell and therefore, prevent the CEO leakage from the millicapsules. This shell has more active
369 calcium-binding sites (G-blocks) with higher degree of cross-linking. (Piornos, et al., 2017). A
370 similar trend could be observed for LC (**Fig. 2, D**). Surface tension and interfacial tension are
371 considered as holding forces, while gravitational and drag forces are assumed as detaching forces
372 of the core-shell droplet at the tip of millifluidic tube. Furthermore, surface tension and
373 gravitational forces are exerted on the continuous phase droplets (shell), but interfacial tension

and drag forces affected the dispersed phase droplets (core) (Chan, Lee, Ravindra, & Poncelet, 2009; Farahmand, et al., 2021; X. Wang, Zhu, Shao, Luo, & Zhang, 2019). The drag force (as a detaching force) is proportional to the continuous phase viscosity. Augmentation of alginate concentration, and also its viscosity exerted higher drag force on the dispersed phase (Martins, et al., 2017). Hence, the small CEO-loaded droplets detached more quickly from the tube. Subsequently, the small millicapsules in gelling bath contained high CEO content compared to their total weight. This is because of the different transferring speed of CEO and viscous alginate, so the LC of millicapsule improved.

When the alginate flow rate (Q_{Alg}) was maintained fixed at the central value, increasing the flow rate of CEO (Q_{CEO}) up to 0.7 mL/min resulted in improved EE (**Fig. 2, B**). However, the higher values of 0.7 mL/min exhibited a reverse effect. Higher density of CEO than alginate solution (1035 and 1001 kg/m^3, respectively) led to faster transferring of CEO in tube. In addition to density, shear stress of the tube wall could reduce the velocity of the alginate solution (Akbari, Rahimi, & Fattahi, 2017) and therefore, CEO flow rates higher than 0.7 mL/min led to a failure in oil entrapping. The LC is the millicapsule ability in CEO loading based on the amount of polymer used. The amount of entrapped CEO in the millicapsules was directly related to the flow rate. The higher flow rates, the more injection of CEO into the droplet compared to the shell solution and therefore, the higher LC (**Fig. 2, E, F**).

As shown in **Fig. 2 (C)**, high flow rates of alginate were desirable for obtaining high EE values. As mentioned above, the CEO droplets moved faster than alginate in the tube. By increasing the alginate flow rate, formation speed of the alginate droplets also enhanced. Consequently, the gravitational force became dominant, which led to successful encapsulation of CEO droplets. An inverse trend was observed concerning to LC as a function of alginate flow rate (**Fig. 2, F**). Increasing the flow rate of the continuous phase affects the gravitational force on the droplets, which helps faster detaching of small droplets from the tube (Cramer, Fischer,

399 & Windhab, 2004). It seems that the high flow rates of alginate caused the higher shell/oil ratio
400 (w/w) in the produced millicapsule. The reduction of required volume of oil loading occurred
401 via more injection of alginate solution, which led to a decrease in LC. (**Fig. 2, F**). As reported
402 by Chan (2011), oil content of calcium alginate beads produced by extrusion-dripping method
403 was reduced at higher ratios (w/w) of shell to oil.
404
405 **Insert figure.2 about here**
406
407
408 **3.2.2. Effect of independent variables on size**
409 The diameter of the millicapsules varied from 3.46 to 3.99 mm (**Fig. 3 A-C**). A converse
410 effect of alginate flow rate on the millicapsules diameter was shown in **Fig. 3. A.** The higher
411 flow rate of alginate induces higher pressure on the interface of two phases, and also a high
412 velocity gradient. As a result, a high drag force acting on the dispersed phase resulted in its
413 breakup into the smaller droplets (T. Fu, Wu, Ma, & Li, 2012). Similar results also were observed
414 by Akbari, et al. (2017)
415 Increasing the alginate concentration from 20 to 30 g/L caused a reduction in millicapsule
416 diameter (from 3.99 to 3.59 mm) (**Fig. 3, B**). This may be due to viscosity increasing of the
417 continuous phase surrounding the CEO droplets inside the tube. Hence, high viscosity of alginate
418 could restrict the fast transfer speed of the CEO and also reduces the interfacial tension as the
419 holding force of oil droplets (Chan, 2011). The reduction of interfacial tension resulted in
420 dominating the detached forces (drag and gravitational), so smaller droplets separated more
421 quickly. As a result, smaller millicapsules produced in the gelling bath.
422 As depicted in **Fig.3, C**, increasing the CEO flow rate from 0.6 to 0.8 mL/min had a
423 positive effect on the millicapsules diameter. Higher flow rate of the inner fluid compared to the
424 continuous phase results in a larger droplet by reducing the shear stress imposed on the inner

phase (Ren, Ju, Xie, & Chu, 2010). The higher values of density and CEO flow rate resulted in more core material enters into the droplet compared to the shell. Inducing more resistance to the continuous phase as a result of the injection inertia of the dispersed phase at high flow rate produces larger droplets (T. Fu, et al., 2012),. Similar results were reported by W. Wang, Waterhouse, and Sun-Waterhouse (2013) for canola oil.

Insert figure.3 about here

3.2.3. Effect of independent variables on SF

As demonstrated in **Fig.3, D**, increasing the alginate pump speed helped to produce a more spherical millicapsule. There are two stages in droplet detaching from the tip of tube: squeezing stage with slight decrease in the thinning rate of the neck (reason of droplet formation with irregular shape) and pinching-off stage with rapid thinning rate. The squeezing stage is function of continuous flow rate. It was mentioned that the rate of neck thinning in the squeezing stage increases as the continuous flow rate enhances. This is due to improving the drag force, which detaches the droplet neck (Pan, Chen, Zhang, & Li, 2020). The impinging velocity of the droplet with the surface of the $CaCl_2$ bath is determining the shape of the produced capsule. In other words, irregular-shaped capsules are formed at a low velocity of collision (Gao, He, Fu, Qiu, & Jin, 2016). Increasing the alginate flow rates and also the gravitational force enabled the droplet to faster detaching. As a result, collision dynamics did not affect the final shape of produced millicapsule.

By increasing the alginate concentration from 20 to 30 g/L the more spherical millicapsule were produced, and the SF increased from 0.94 to 0.97 (**Fig. 3, E**). It seems the core-shell droplets from dilute alginate solution are mostly unable to retain sphericity during

cross-linking stage by restoring forces (interfacial tension and hydrostatic pressure) or against the drag force upon collision with the surface of calcium chloride bath (Lee, Ravindra, & Chan, 2013). Hence, irregular-shaped millicapsules were observed at lower concentrations of alginate.

As illustrated in **Fig. 3, F**, increasing the CEO flow rate resulted in a decrease in the sphericity. The shape evolution of millicapsules depends on the competition between the cross-linking process and the fluid drag force. Deformation of the droplet is highly affected by the drag enforced by the gelling bath (Haldar & Chakraborty, 2018). The entrance of the dispersed phase (CEO) in a large volume into the droplet would lead to a thin shell with less cross-linking degree. This droplet could not tolerate the fluid drag force; therefore, irregular-shaped millicapsules would produce.

3.2.4. Optimization of variables and verification of design

Since the encapsulation efficiency and sphericity values were appropriate in all experimental runs, the optimized encapsulation process was selected based on achieving the EE and SF values in range, the maximum LC, and the minimum diameter of millicapsules using the numerical point prediction method. The optimized conditions included the alginate concentration of 30 g/L, alginate flow rate of 1.09 mL/min, and CEO flow rate of 0.8 mL/min. Desirability as accuracy criterion in the optimized conditions was 0.91, which is quite close to 1. The predicted EE, LC, SF, and size values were 98.11%, 71.46%, 0.97, and 3.52 mm, respectively, while the values for the optimized conditions were measured as 98.96± 1.2%, 70.14± 1.8%, 0.96± 0.01, and 3.58± 0.23 mm. These results corresponded well with the predicted data approving that the regression model was adequate for prediction of the millifluidic encapsulation of CEO.

The literature review showed that the millifluidic method compared to other oil-core encapsulation techniques exhibited higher efficiency and ability to produce spherical millicapsules (Chew & Nyam, 2016; S. Y. Koo, Cha, Song, Chung, & Pan, 2014; Morales, et

476 al., 2017; Sittipummongkol, Chuysinuan, Techasakul, Pisitsak, & Pechyen, 2019; Volić, et al.,
477 2018).

478 The dripping flow pattern of the droplet formation in the tube was shown in **Fig. 4**.
479 Droplet formation occurs directly after the two phases meet in the dripping process. **Fig. 4 (C)**,
480 demonstrated the optimal millicapsules at the time of falling into the bath and after 30 min
481 gelation (**Fig. 4, D**).

482

483 **Insert figure.4 about here**

484

485 **3.3. Characterization of optimal millicapsules**

486 **3.3.1. Mechanical stability**

487 The alginate millicapsules undergo mechanical stress caused by compression, osmotic pressure,
488 and shear forces during food processing. The diameter of millicapsules, amount of core loading,
489 cross-linking time, strength, and the degree of the cross-linking exhibit a considerable effect on
490 the mechanical stiffness. Alginate millicapsules are sensitive to deformation, rupture, and even
491 undesirable early release of the core. Hence, the optimal millicapsules was coated with a chitosan
492 layer for further analysis. The Young modulus values of the coated millicapsules as a function
493 of chitosan concentration is plotted in **Fig**. **5**. The millicapsules coated with chitosan
494 concentrations higher than 0.5% w/v were stronger than the millicapsules without coating. There
495 was not a significant difference ($p<0.05$) between the Young moduli of uncoated samples and
496 the millicapsules coated with 0.25% w/v chitosan concentration (**Fig. 5**). The highest value of
497 Young modulus and the mechanical stability was achieved at 1.5% w/v chitosan (16×10^5 Pa),
498 which was approximately 1.76 times higher than uncoated millicapsules (9.1×10^5 Pa) (**Fig.5**).
499 This can be translated into the strong electrostatic interactions between amino groups of chitosan
500 and carboxyl groups of alginate due to the reticulation of GG and MG blocks of alginate with

501 Ca^{2+} and the formation of cooperative ionic bonds between the M residues with the protonated
502 amino groups of chitosan (Dupuy, Arien, & Minnot, 1994). Similar results were also reported
503 by Bedade, Sutar, and Singhal (2019). Consequently, the optimal millicapsules were coated with
504 1.5% w/v chitosan concentration.
505
506 **Insert figure.5 about here**
507
508 **3.3.2. Surface morphology**
509 The surface morphology of coated and uncoated millicapsules containing CEO was
510 assessed using scanning electron microscopy (**Fig. 6, a-f**). The micrographs (**Fig6, c, d**)
511 exhibited small dents and rough external surface with many wrinkles on the matrix of the
512 uncoated millicapsules. However, coating the millicapsules with chitosan drastically reduced
513 the surface fissures and holes, making it rigid, smooth and dense (**Fig. 6, e, f**). Compared to
514 the uncoated millicapsules, this structure provides a higher degree of core protection via the
515 permeability reduction. Improving the mechanical strength of the chitosan-coated capsule was
516 also reported by Sun, et al. (2020).
517
518
519 **Insert figure.6 about here**
520
521
522 **3.3.3. Thermal properties**
523 DSC curves of the pure CEO, shell materials, the unloaded, the CEO-loaded, and the
524 chitosan-coated optimal millicapsules are depicted in **Fig. 7**. A broad endothermic peak at 78 °C
525 associated with water loss and a sharp exothermic peak at 245.32 °C attributed to polymer chains
526 decomposition were demonstrated in DSC curve of alginate powder (**Fig. 7, a**). The thermal

characteristics of pure CEO were also investigated by DSC thermograms (**Fig. 7, b**). Two endothermic peaks at 48.1 °C and 195.4 °C were detected, which assigned the evaporation of the residual solvent in essential oil and CEO degradation, respectively. It is worth mentioning that the residual solvent was not detected in the GC-MS chromatogram due to the delay-time of the dilution step with acetone (See section 2.2). According to Süfer and Bozok (2020), endothermic pattern of essential oil thermogram is strongly associated with double bonds and an indicator of decomposition. Shao, Yu, Chen, and Gao (2021) and Yang, et al. (2021) reported the degradation temperature of CEO as 159 °C and 166.26 °C, respectively. Evaluation of thermal properties approved the heat sensitivity and volatile nature of CEO. Elimination of absorbed water in chitosan powder was evident at 77 °C endothermic peak and a sharp exothermic peak at 295.21 °C revealed the decomposition onset of chitosan chains. The "egg-box" structure formation with calcium ions resulted in disappearing of the exothermic peak in the DSC thermogram of calcium-alginate (unloaded) millicapsules (**Fig. 7, d**) (Lupo, Maestro, Gutiérrez, & González, 2015).

There were two sharp endothermic peaks corresponded to loss of bound water in the thermograms of uncoated millicapsules (**Fig. 7, d, e**), which were disappeared in the chitosan-coated millicapsules due to complete coverage (**Fig 7, f**). Chitosan-alginate reaction can be confirmed by disappearing the exothermic peaks of pure chitosan and alginate (**Fig 7, a, c, f**) (Sankalia, Mashru, Sankalia, & Sutariya, 2007). As demonstrated in **Fig. 7, f**, there was only an endothermic characteristic peak at 225.7 °C, which was shifted to higher temperatures than the CEO thermogram. Furthermore, the evaporation peak of the residual solvent in CEO at 48.1 °C (**Fig. 7, b**) has disappeared in the thermograms of chitosan-coated and CEO-loaded millicapsules (**Fig. 7, e, f**). This revealed the successful incorporation of essential oil in encapsulating polymer and also higher thermal stability of encapsulated CEO. Besides, the absence of additional peaks for millicapsules compared to the pure samples pointed no interactions among CEO/ alginate/ chitosan (Hadidi, Pouramin, Adinepour, Haghani, & Jafari, 2020).

552

553 **Insert figure.7 about here**

554

555 **3.3.4. FTIR**

556 The FTIR analysis confirmed the presence of core, shell component, and the interaction
557 between the chitosan and shell layer, as highlighted in **Fig**. **8**. As shown in **Fig.8, a,**
558 characteristic absorption bands of alginate powder at 3433 cm^{-1} (stretching vibration of OH),
559 2924 cm^{-1} (CH), 1629 cm^{-1} (COO^-, asymmetric), and 1029 cm^{-1} (C-O-C) were similar to other
560 researches (Angadi, Manjeshwar, & Aminabhavi, 2012; Daemi & Barikani, 2012). CH2-
561 stretching vibration of the pure CEO was observed at 2814 cm^{-1} (**Fig.8, b**). Characteristic
562 absorption peaks at 1677 and 1625 cm^{-1} were associated with aldehyde carbonyl (C=O
563 stretching vibration) and also the presence of the cinnamaldehydes and aldehydes in the
564 essential oil. Other peaks around 1575 and 1124 cm^{-1} were related to the aromatic ring (C=O
565 skeleton vibration) and C-O deformation vibration, respectively (de Oliveira, Paula, & de Paula,
566 2014). The bands such as those at 1450 and 1294 cm^{-1} originated from various organic
567 compounds verified in the CEO by GC/MS analysis (see **Table 2**). The FTIR spectrum of
568 chitosan powder (**Fig.8, c**) demonstrated the characteristic bands at 3436, 2873, 1660, 1580,
569 1422, 1381, 1159, and 895 cm^{-1} that corresponded to OH stretching, C-H stretching, C=O
570 stretching of amide I, bending vibrations of N-H in N-acetylated residues, N-H stretching of
571 amide II, N-H stretching of amide III, C-O-C stretching, and pyranose ring, respectively
572 (Hasheminejad, Khodaiyan, & Safari, 2019).

573 Incorporation of the CEO in the calcium-alginate millicapsules (**Fig. 8, e**) led to a higher
574 intensity for the CH stretching peak at 2855 cm^{-1}, which was associated with the CEO ester
575 groups (Hosseini, et al., 2013). Furthermore, similar peaks of the CEO and CEO-loaded spectra
576 with minor differences revealed the successful entrapment of the CEO in the millicapsules

without interaction with the alginate matrix. The spectra of CEO-loaded and chitosan-CEO-loaded millicapsules (**Fig. 8, e, f**) showed many similarities with the CEO spectrum (**Fig. 8, b**). However, due to the millicapsules and CEO bands overlapping, some small variations in the intensities and the shapes of the bands were observed. Sharpening of the peak at 1625 cm^{-1} due to the alginate carboxyl groups and disappearance of the bands at 1580 cm^{-1} revealed the formation of electrostatic interactions between chitosan and alginate (Lai, Lin, Mo, Xu, & Lin, 2017).

Insert figure.8 about here

3.3.5. Crystallinity

Products of microencapsulation process with crystalline structure tend to dissolve slowly in solution due to the dissolution of surface crystals which exposed to solvent (de Barros Fernandes, et al., 2016). Hence, XRD analysis was performed to confirm the successful encapsulation of CEO in the chitosan-loaded millicapsules and its impact on the physical state of shell materials. The alginate powder (**Fig. 9, a**) exhibited some characteristic peaks at 13.5 °, 23.17 °, 24.19 °, 26.67 °, 30.19 °, and 36.75 ° (2θ), which showed the semi-crystallinity structure of alginate (Lakouraj, Mojerlou, & Zare, 2014). The diffraction spectrum of the chitosan powder showed a weak and a strong peak at 2θ of 11 ° and 20.14 °, respectively (**Fig. 9, b**). These peaks represented that chitosan had two different forms of crystal morphologies. The first peak is related to hydrated forms and the next one corresponds to a more regular anhydrous form (Ogawa, Yui, & Miya, 1992).

No peak was shown in the diffractogram of unloaded and chitosan-unloaded millicapsules (**Fig. 9, c, d**), which is implied destruction of the crystalline structure of the alginate and chitosan during ionic gelation and electrostatic binding, respectively. In other words, complexion of the

chitosan and alginate resulted in slowing down the formation of the hydrogen bonds among amino groups and hydroxyl groups, so a sharp peak of the chitosan powder disappeared. Furthermore, the chitosan-unloaded millicapsules showed an amorphous morphology (Liang, Liu, & Wu, 2007; Lim & Ahmad, 2017). The disappearance of the exothermic peaks of chitosan and alginate proved the successful interaction between the two biopolymers. This result implies the transformation possibility of the crystal to amorphous structure (Crcarevska, Dodov, & Goracinova, 2008). As compared with chitosan-unloaded millicapsule, the characteristic peak at 2θ of 23 ° in the X-ray diffraction pattern of CEO-loaded millicapsule confirmed the CEO entrapping in the chitosan-millicapsules (**Fig. 9, f**). Accordingly, it is obvious that the incorporation of CEO might result in the disarray of the chitosan-coated millicapsules packing structure. A similar transition from crystalline form to amorphous has already been observed recently (Bagheri, Ariaii, & Motamedzadegan, 2020; Hosseini, et al., 2013; Matshetshe, Parani, Manki, & Oluwafemi, 2018).

Insert figure.9 about here

3.3.6. In vitro digestion and release kinetic in the simulated gastrointestinal tract (GIT)

The release behavior of the CEO from the optimal coated and uncoated (control) millicapsules in the mouth (2 min), stomach (120 min), and small intestine (120 min) is depicted in **Fig. 10**. As shown in the figure, only a small amount of CEO (2.06 %) was released from coated millicapsules in the SSF. This was attributed to the short-time of exposure to simulated saliva system and coating matrix. However, unlike the oral phase, rate of the CEO release from coated millicapsule reached to 27.38 % in SGF (**Fig. 10**). The intense acidic condition (pH= 2.5) and existence of pepsin enzyme in the SGF could promote the release from millicapsules, but it was obvious that chitosan coating retarded the CEO release rate. The electrostatic interaction

between amino groups of chitosan and carboxylic groups of alginate play an important role in retarding the release rate (Luo & Wang, 2014). At the end of this stage, 72.62 % of the CEO was preserved in the coated millicapsules. The higher and faster release of CEO from coated millicapsules was observed in the small intestine (**Fig. 10**). The CEO release was increased during exposure time in SIF, which coated millicapsules released 77.96 % of its loaded oil during passing 240 min in GI tract phases. The fast release of CEO was associated with the high number of digested millicapsules. As a result, entrapped CEO in the partially digested millicapsules was released further in the SIF (pH= 7) due to the effect of pancreatin enzyme on wall material (J. Fu, et al., 2020). The CEO-loaded millicapsules with chitosan coating can assuredly be applied as intestinal site-specific delivery system, because of its pH-dependent behavior in targeted release.

According to **Fig. 10**, 7.06 % of CEO was released from the control sample into SSF (during the first 2 min of digestion). However, about 66.8 % of CEO was leached from the control sample into SGF, which was 2.5 times higher than the coated millicapsules leakage. In the intestine stage, the CEO loaded in the control sample was completely released during 40 min and the millicapsules were digested. Lack of chitosan coating led to the fast release of CEO in the acidic conditions of stomach (**Fig. 10**).

Insert figure.10 about here

The model-fitting kinetics of the CEO release from coated and uncoated millicapsules with various models (Higuchi, Ritger-Peppas, Korsmeyer-Peppas, and Kopcha) revealed that the Ritger-Peppas model was regarded as the most suitable model for describing the mechanism of CEO release in coated millicapsules. The mentioned model showed the highest R^2 and the lowest RMSE values compared to the other models in all digestion phases of coated millicapsules (**Table 4**). In Ritger-Peppas model, the n value presents the release mechanism of essential oil. According

to **Table 4**, for coated millicapsules the n parameter in mouth and small intestine phases were higher than 0.85, indicating that the dominant mechanism was non-Fickian diffusion (super case II) as an extreme type of transfer. In the stomach phase, the n value of millicapsule was between 0.43 and 0.85 (**Table 4**), denoting non-Fickian diffusion (anomalous transport) (Ritger, et al., 1987).

Basically, three important phenomena happen during the contact of medium with the millicapsules: diffusion, swelling and erosion. From the mathematical point of view, these processes could be described using two models: Fickian (case I) and non-Fickian (case II, Anomalous Case, and Super Case II) (Malekjani & Jafari, 2021). In this study, swelling and polymeric chain relaxation (disentanglement of the matrix) were the main release mechanisms during the contact of millicapsules with SGF (anomalous transport), so that, SGF penetrated rapidly into the structure of the millicapsules, while the matrix slowly dissolved into the SGF (pH=2.5). The thickness of the matrix enhanced due to the SGF uptake and consequently, disentanglement of the polymeric chain occurred.

Furthermore, $|A/B|<1$ in the Kopcha model of coated millicapsules in the three phases indicated the matrix erosion (Kopcha, et al., 1990). In this case, the degradation rate of the matrix was much faster than the penetration of the medium into the polymeric structure (Malekjani & Jafari, 2021).

Noppakundilograt, Piboon, Graisuwan, Nuisin, and Kiatkamjornwong (2015) also proposed Ritger-Peppas model with non-Fickian transport as the best model of release mechanism of eucalyptus oil from alginate microcapsule. Ritger-Peppas model was selected as the most suitable model in mouth and small intestine for the control sample. However, Kopcha was the best model to describe the release of CEO from the uncoated millicapsules in the stomach. The n values of the Ritger-Peppas model in mouth and small intestine stages denoted non-Fickian

677 diffusion (anomalous transport in mouth and super case II in small intestine). |A/B|>1 of Kopcha
678 model in the stomach stage of the control sample represented Fickian diffusion (Kopcha, et al.,
679 1990).

680

681 **Insert table.4 about here**

682

683 **4. Conclusion**

684 In this work, the CEO was encapsulated using millifluidic device and RSM was applied
685 for assessing the effects of the independent variables on the EE, LC, size, and SF of the produced
686 millicapsules. The results showed that all three variables had significant effects ($p< 0.05$) on the
687 responses. The optimal millimeter-scale capsule (3.58± 0.23 mm) had the highest EE (98.96±
688 1.2%) and LC (70.14± 1.8%) values and it could be considered as a completely round
689 millicapsules (SF= 0.96± 0.01). The chitosan-coating layer (at 1.5% w/v concentration) created
690 the highest mechanical stability in the millicapsules. Surface fissures, pleats, and holes were
691 disappeared in the SEM image of the coated millicapsules. Endothermic peak in the chitosan-
692 CEO- loaded millicapsules was shifted to the higher temperatures, which highlighted the higher
693 thermal stability of the encapsulated CEO. Similar peaks with minor differences in the FTIR
694 spectrums of free CEO and its encapsulated form also confirmed the successful entrapment
695 without any chemical interaction with the shell matrix. Transition of the crystalline form of pure
696 materials to the amorphous form of millicapsules also proved the proper incorporation of the
697 CEO. Release kinetics of cinnamon essential oil in the simulated conditions of GIT followed a
698 non-Fickian mechanism. Ritger-Peppas model was selected as the most suitable model to predict
699 the essential oil release from coated millicapsules. However, Fickian diffusion was observed for
700 uncoated millicapsules in stomach. Concerning to the results, the designed millicapsules could

be considered as promising delivery system for well-controlling the CEO release and would be a good choice for intestinal site-specific delivery system.

References

Adorjan, B., & Buchbauer, G. (2010). Biological properties of essential oils: an updated review. *Flavour and Fragrance Journal, 25*(6), 407-426.

Akamatsu, K., & Yamaguchi, T. (2007). Novel preparation method for obtaining pH-responsive core-shell microcapsule reactors. *Industrial and Engineering Chemistry Research 46*(1), 124-130.

Akbari, M., Rahimi, M., & Fattahi, A. (2017). Evaluation of microparticles formation by external gelationin a microfluidic system. *Chemical Engineering and Processing: Process Intensification, 117*, 171-178.

Angadi, S. C., Manjeshwar, L. S., & Aminabhavi, T. M. (2012). Novel composite blend microbeads of sodium alginate coated with chitosan for controlled release of amoxicillin. *International Journal of Biological Macromolecules 51*(1-2), 45-55.

Bagheri, R., Ariaii, P., & Motamedzadegan, A. (2020). Characterization, antioxidant and antibacterial activities of chitosan nanoparticles loaded with nettle essential oil. *Journal of Food Measurement and Characterization*, 1-8.

Baldim, I., Rosa, D. M., Souza, C. R., Ana, R. d., Durazzo, A., Lucarini, M., Santini, A., Souto, E. B., & Oliveira, W. P. (2020). Factors affecting the retention efficiency and physicochemical properties of spray dried lipid nanoparticles loaded with lippia sidoides essential oil. *Biomolecules, 10*(5), 693.

Bastos, L. P. H., de Sá Costa, B., Siqueira, R. P., & Garcia-Rojas, E. E. (2020). Complex coacervates of β-lactoglobulin/sodium alginate for the microencapsulation of black pepper (Piper nigrum L.) essential oil: Simulated gastrointestinal conditions and modeling release kinetics. *International Journal of Biological Macromolecules 160*, 861-870.

Bedade, D. K., Sutar, Y. B., & Singhal, R. S. (2019). Chitosan-coated calcium alginate beads for covalent immobilization of acrylamidase: process parameters and removal of acrylamide from coffee. *Food Chemistry 275*, 95-104.

Caruso, F., Schüler, C., & Kurth, D. G. (1999). Core– shell particles and hollow shells containing metallo-supramolecular components. *Chemistry of Materials, 11*(11), 3394-3399.

Chan, E.-S. (2011). Preparation of Ca-alginate beads containing high oil content: Influence of process variables on encapsulation efficiency and bead properties. *Carbohydrate Polymers 84*(4), 1267-1275.

Chan, E.-S., Lee, B.-B., Ravindra, P., & Poncelet, D. (2009). Prediction models for shape and size of ca-alginate macrobeads produced through extrusion-dripping method. *Journal of Colloid and Interface Science 338*(1), 63-72.

Chan, E.-S., Lim, T.-K., Voo, W.-P., Pogaku, R., Tey, B. T., & Zhang, Z. (2011). Effect of formulation of alginate beads on their mechanical behavior and stiffness. *Particuology, 9*(3), 228-234.

Chen, K., Chen, X., Liang, L., & Xu, X. (2020). Gallic acid-aided cross-linking of myofibrillar protein fabricated soluble aggregates for enhanced thermal stability and a tunable colloidal state. *Journal of agricultural and food chemistry, 68*(41), 11535-11544.

Chen, X., Qiu, Q., Chen, K., Li, D., & Liang, L. (2020). Water-soluble myofibrillar protein–pectin complex for enhanced physical stability near the isoelectric point: Fabrication, rheology and thermal property. *International journal of biological macromolecules, 142*, 615-623.

Chew, S.-C., & Nyam, K.-L. (2016). Microencapsulation of kenaf seed oil by co-extrusion technology. *Journal of Food Engineering, 175*, 43-50.

Cramer, C., Fischer, P., & Windhab, E. J. (2004). Drop formation in a co-flowing ambient fluid. *Chemical Engineering Science 59*(15), 3045-3058.

Crcarevska, M. S., Dodov, M. G., & Goracinova, K. (2008). Chitosan coated Ca–alginate microparticles loaded with budesonide for delivery to the inflamed colonic mucosa. *European Journal of Pharmaceutics and Biopharmaceutics 68*(3), 565-578.

Daemi, H., & Barikani, M. (2012). Synthesis and characterization of calcium alginate nanoparticles, sodium homopolymannuronate salt and its calcium nanoparticles. *Scientia Iranica, 19*(6), 2023-2028.

Davarcı, F., Turan, D., Ozcelik, B., & Poncelet, D. (2017). The influence of solution viscosities and surface tension on calcium-alginate microbead formation using dripping technique. *Food Hydrocolloids, 62*, 119-127.

de Barros Fernandes, R. V., Borges, S. V., Silva, E. K., da Silva, Y. F., de Souza, H. J. B., do Carmo, E. L., de Oliveira, C. R., Yoshida, M. I., & Botrel, D. A. (2016). Study of ultrasound-assisted emulsions on microencapsulation of ginger essential oil by spray drying. *Industrial Crops and Products 94*, 413-423.

de Oliveira, E. F., Paula, H. C., & de Paula, R. C. (2014). Alginate/cashew gum nanoparticles for essential oil encapsulation. *Colloids and Surfaces B: Biointerfaces, 113*, 146-151.

Dupuy, B., Arien, A., & Minnot, A. P. (1994). FT-IR of membranes made with alginate/polylysine complexes. Variations with the mannuronic or guluronic content of the polysaccharides. *Artificial Cells, Blood Substitutes, and Biotechnology, 22*(1), 71-82.

Fadel, H. H., Hassan, I. M., Ibraheim, M. T., Abd El Mageed, M. A., & Saad, R. (2019). Effect of using cinnamon oil encapsulated in maltodextrin as exogenous flavouring on flavour quality and stability of biscuits. *Journal of Food Science and Technology 56*(10), 4565-4574.

Farahmand, A., Emadzadeh, B., Ghorani, B., & Poncelet, D. (2021). A comprehensive parametric study for understanding the combined millifluidic and dripping encapsulation process and characterisation of oil-loaded capsules. *Journal of Microencapsulation*, 1-15.

Fery, A., & Weinkamer, R. (2007). Mechanical properties of micro-and nanocapsules: Single-capsule measurements. *Polymer, 48*(25), 7221-7235.

Fu, J., Song, L., Liu, Y., Bai, C., Zhou, D., Zhu, B., & Wang, T. (2020). Improving oxidative stability and release behavior of docosahexaenoic acid algae oil by microencapsulation. *Journal of the Science of Food and Agriculture 100*(6), 2774-2781.

Fu, T., Wu, Y., Ma, Y., & Li, H. Z. (2012). Droplet formation and breakup dynamics in microfluidic flow-focusing devices: from dripping to jetting. *Chemical Engineering Science 84*, 207-217.

Galanakis, C. M. (2020). The food systems in the era of the coronavirus (COVID-19) pandemic crisis. *Foods, 9*(4), 523.

Galanakis, C. M. (2021). Functionality of food components and emerging technologies. *Foods, 10*(1), 128.

Gao, Q., He, Y., Fu, J.-z., Qiu, J.-j., & Jin, Y.-a. (2016). Fabrication of shape controllable alginate microparticles based on drop-on-demand jetting. *Journal of Sol-Gel Science and Technology, 77*(3), 610-619.

Gholamian, S., Nourani, M., & Bakhshi, N. (2020). Formation and characterization of calcium alginate hydrogel beads filled with cumin seeds essential oil. *Food Chemistry 338*, 128143.

Gong, C., Lee, M. C., Godec, M., Zhang, Z., & Abbaspourrad, A. (2020). Ultrasonic encapsulation of cinnamon flavor to impart heat stability for baking applications. *Food Hydrocolloids, 99*, 105316.

Gorbunova, N., Evteev, A., Evdokimov, I., & BANNIKOVA, A. (2016). Kinetics of ascorbic acid transport from alginate beads during in vitro digestion. *Journal of Food & Nutrition Research, 55*(2).

Granato, D., Barba, F. J., Bursać Kovačević, D., Lorenzo, J. M., Cruz, A. G., & Putnik, P. (2020). Functional foods: Product development, technological trends, efficacy testing, and safety. *Annual Review of Food Science and Technology, 11*, 93-118.

Granato, D., Nunes, D. S., & Barba, F. J. (2017). An integrated strategy between food chemistry, biology, nutrition, pharmacology, and statistics in the development of functional foods: A proposal. *Trends in Food Science & Technology, 62*, 13-22.

Hadidi, M., Pouramin, S., Adinepour, F., Haghani, S., & Jafari, S. M. (2020). Chitosan nanoparticles loaded with clove essential oil: Characterization, antioxidant and antibacterial activities. *Carbohydrate Polymers* 116075.

Haldar, K., & Chakraborty, S. (2018). Role of chemical reaction and drag force during drop impact gelation process. *Colloids and Surfaces A: Physicochemical and Engineering Aspects, 559*, 401-409.

Hasheminejad, N., Khodaiyan, F., & Safari, M. (2019). Improving the antifungal activity of clove essential oil encapsulated by chitosan nanoparticles. *Food Chemistry 275*, 113-122.

Higuchi, T. (1963). Mechanism of sustained-action medication. Theoretical analysis of rate of release of solid drugs dispersed in solid matrices. *Journal of pharmaceutical sciences, 52*(12), 1145-1149.

Hosseini, S. F., Zandi, M., Rezaei, M., & Farahmandghavi, F. (2013). Two-step method for encapsulation of oregano essential oil in chitosan nanoparticles: preparation, characterization and in vitro release study. *Carbohydrate polymers, 95*(1), 50-56.

Hu, J., Zhang, Y., Xiao, Z., & Wang, X. (2018). Preparation and properties of cinnamon-thyme-ginger composite essential oil nanocapsules. *Industrial Crops and Products 122*, 85-92.

Hyldgaard, M., Mygind, T., & Meyer, R. L. (2012). Essential oils in food preservation: mode of action, synergies, and interactions with food matrix components. *Frontiers in microbiology, 3*, 12.

Kim, W.-T., Chung, H., Shin, I.-S., Yam, K. L., & Chung, D. (2008). Characterization of calcium alginate and chitosan-treated calcium alginate gel beads entrapping allyl isothiocyanate. *Carbohydrate Polymers 71*(4), 566-573.

Koo, S.-M., Cho, Y.-H., Huh, C.-S., Baek, Y.-J., & Park, J.-Y. (2001). Improvement of the stability of Lactobacillus casei YIT 9018 by microencapsulation using alginate and chitosan. *Journal of Microbiology and Biotechnology, 11*(3), 376-383.

Koo, S. Y., Cha, K. H., Song, D. G., Chung, D., & Pan, C. H. (2014). Microencapsulation of peppermint oil in an alginate–pectin matrix using a coaxial electrospray system. *International Journal of Food Science & Technology 49*(3), 733-739.

Kopcha, M., Tojo, K. J., & Lordi, N. G. (1990). Evaluation of methodology for assessing release characteristics of thermosoftening vehicles. *Journal of Pharmacy and Pharmacology 42*(11), 745-751.

Korsmeyer, R. W., Gurny, R., Doelker, E., Buri, P., & Peppas, N. A. (1983). Mechanisms of solute release from porous hydrophilic polymers. *International Journal of Pharmaceutics, 15*(1), 25-35.

Lai, F., Lin, B., Mo, F., Xu, C., & Lin, M. (2017). Novel composite microparticles of alginate coated with chitosan for controlled release and protection of ascorbic acid. *Advances in Polymer Technology, 36*(1), 58-67.

Lakouraj, M. M., Mojerlou, F., & Zare, E. N. (2014). Nanogel and superparamagnetic nanocomposite based on sodium alginate for sorption of heavy metal ions. *Carbohydrate Polymers 106*, 34-41.

Lee, B. B., Ravindra, P., & Chan, E. S. (2013). Size and shape of calcium alginate beads produced by extrusion dripping. *Chemical Engineering & Technology, 36*(10), 1627-1642.

Li, J., Kim, S. Y., Chen, X., & Park, H. J. (2016). Calcium-alginate beads loaded with gallic acid: Preparation and characterization. *LWT-Food Science and Technology, 68*, 667-673.

Li, W., Zhang, L., Ge, X., Xu, B., Zhang, W., Qu, L., Choi, C.-H., Xu, J., Zhang, A., & Lee, H. (2018). Microfluidic fabrication of microparticles for biomedical applications. *Chemical Society Reviews, 47*(15), 5646-5683.

Liang, R., Liu, M., & Wu, L. (2007). Controlled release NPK compound fertilizer with the function of water retention. *Reactive and Functional Polymers, 67*(9), 769-779.

Lim, G.-P., & Ahmad, M. S. (2017). Development of Ca-alginate-chitosan microcapsules for encapsulation and controlled release of imidacloprid to control dengue outbreaks. *Journal of Industrial and Engineering Chemistry 56*, 382-393.

Liouni, M., Drichoutis, P., & Nerantzis, E. T. (2008). Studies of the mechanical properties and the fermentation behavior of double layer alginate–chitosan beads, using Saccharomyces cerevisiae entrapped cells. *World Journal of Microbiology and Biotechnology, 24*(2), 281-288.

Luo, Y., & Wang, Q. (2014). Recent development of chitosan-based polyelectrolyte complexes with natural polysaccharides for drug delivery. *International Journal of Biological Macromolecules 64*, 353-367.

Lupo, B., Maestro, A., Gutiérrez, J. M., & González, C. (2015). Characterization of alginate beads with encapsulated cocoa extract to prepare functional food: comparison of two gelation mechanisms. *Food Hydrocolloids, 49*, 25-34.

Malekjani, N., & Jafari, S. M. (2021). Modeling the release of food bioactive ingredients from carriers/nanocarriers by the empirical, semiempirical, and mechanistic models. *Comprehensive Reviews in Food Science and Food Safety, 20*(1), 3-47.

Martins, E., Poncelet, D., Marquis, M., Davy, J., & Renard, D. (2017). Monodisperse core-shell alginate (micro)-capsules with oil core generated from droplets millifluidic. *Food Hydrocolloids, 63*, 447-456.

Matshetshe, K. I., Parani, S., Manki, S. M., & Oluwafemi, O. S. (2018). Preparation, characterization and in vitro release study of β-cyclodextrin/chitosan nanoparticles loaded Cinnamomum zeylanicum essential oil. *International Journal of Biological Macromolecules 118*, 676-682.

Minekus, M., Alminger, M., Alvito, P., Ballance, S., Bohn, T., Bourlieu, C., Carriere, F., Boutrou, R., Corredig, M., & Dupont, D. (2014). A standardised static in vitro digestion method suitable for food–an international consensus. *Food & Function 5*(6), 1113-1124.

Morales, E., Rubilar, M., Burgos-Díaz, C., Acevedo, F., Penning, M., & Shene, C. (2017). Alginate/Shellac beads developed by external gelation as a highly efficient model system for oil encapsulation with intestinal delivery. *Food Hydrocolloids, 70*, 321-328.

Muhammad, D. R. A., Doost, A. S., Gupta, V., bin Sintang, M. D., Van de Walle, D., Van der Meeren, P., & Dewettinck, K. (2020). Stability and functionality of xanthan gum–shellac nanoparticles for the encapsulation of cinnamon bark extract. *Food Hydrocolloids, 100*, 105377.

Murata, Y., Maeda, T., Miyamoto, E., & Kawashima, S. (1993). Preparation of chitosan-reinforced alginate gel beads—effects of chitosan on gel matrix erosion. *International Journal of Pharmaceutics, 96*(1-3), 139-145.

Noghabi, M. S., & Molaveisi, M. (2020). Microencapsulation of Persian gum as a novel wall material for the fast-release of cinnamon essential oil in the simulated saliva medium: Characterization of microcapsules and modeling the kinetics of release. *Bioactive Carbohydrates and Dietary Fibre*, 100250.

Noppakundilograt, S., Piboon, P., Graisuwan, W., Nuisin, R., & Kiatkamjornwong, S. (2015). Encapsulated eucalyptus oil in ionically cross-linked alginate microcapsules and its controlled release. *Carbohydrate polymers, 131*, 23-33.

Ogawa, K., Yui, T., & Miya, M. (1992). Dependence on the preparation procedure of the polymorphism and crystallinity of chitosan membranes. *Bioscience, Biotechnology, and Biochemistry 56*(6), 858-862.

Pan, D., Chen, Q., Zhang, Y., & Li, B. (2020). Investigation on millimeter-scale W1/O/W2 compound droplets generation in a co-flowing device with one-step structure. *Journal of Industrial and Engineering Chemistry 84*, 366-374.

Paris, M., Ramirez-Corona, N., Palou, E., & López-Malo, A. (2020). Modelling release mechanisms of cinnamon (Cinnamomum zeylanicum) essential oil encapsulated in alginate beads during vapor-phase application. *Journal of Food Engineering*, 110024.

Parris, N., Cooke, P. H., & Hicks, K. B. (2005). Encapsulation of essential oils in zein nanospherical particles. *Journal of Agricultural and Food Chemistry 53*(12), 4788-4792.

Pendyala, G., Bithi, S., Vanapalli, S., & Fernandes, G. (2019). Continuous and high throughput production of alginate fibers using co-flow in a millifluidic T-junction. *Journal of Applied Polymer Science, 136*(9), 47120.

Pereda, M., Poncelet, D., & Renard, D. (2019). Characterization of Core-Shell Alginate Capsules. *Food Biophysics, 14*(4), 467-478.

Phawaphuthanon, N., Behnam, S., Koo, S. Y., Pan, C.-H., & Chung, D. (2014). Characterization of core–shell calcium-alginate macrocapsules fabricated by electro-coextrusion. *International journal of biological macromolecules, 65*, 267-274.

907 Piornos, J. A., Burgos-Díaz, C., Morales, E., Rubilar, M., & Acevedo, F. (2017). Highly efficient
908 encapsulation of linseed oil into alginate/lupin protein beads: Optimization of the emulsion
909 formulation. *Food Hydrocolloids, 63*, 139-148.
910 Ponrasu, T., Yang, R.-F., Chou, T.-H., Wu, J.-J., & Cheng, Y.-S. (2020). Core-Shell Encapsulation of
911 Lipophilic Substance in Jelly Fig (Ficus awkeotsang Makino) Polysaccharides Using an
912 Inexpensive Acrylic-Based Millifluidic Device. *Applied Biochemistry and Biotechnology 191*(1),
913 360-375.
914 Purwanti, N., Zehn, A. S., Pusfitasari, E. D., Khalid, N., Febrianto, E. Y., Mardjan, S. S., Andreas, &
915 Kobayashi, I. (2018). Emulsion stability of clove oil in chitosan and sodium alginate matrix.
916 *International Journal of Food Properties 21*(1), 566-581.
917 Radünz, M., da Trindade, M. L. M., Camargo, T. M., Radünz, A. L., Borges, C. D., Gandra, E. A., &
918 Helbig, E. (2019). Antimicrobial and antioxidant activity of unencapsulated and encapsulated
919 clove (Syzygium aromaticum, L.) essential oil. *Food Chemistry 276*, 180-186.
920 Ren, P.-W., Ju, X.-J., Xie, R., & Chu, L.-Y. (2010). Monodisperse alginate microcapsules with oil core
921 generated from a microfluidic device. *Journal of Colloid and Interface Science 343*(1), 392-395.
922 Ritger, P. L., & Peppas, N. A. (1987). A simple equation for description of solute release I. Fickian and
923 non-fickian release from non-swellable devices in the form of slabs, spheres, cylinders or discs.
924 *Journal of Controlled Release, 5*(1), 23-36.
925 Sangsuwan, J., Pongsapakworawat, T., Bangmo, P., & Sutthasupa, S. (2016). Effect of chitosan beads
926 incorporated with lavender or red thyme essential oils in inhibiting Botrytis cinerea and their
927 application in strawberry packaging system. *LWT, 74*, 14-20.
928 Sankalia, M. G., Mashru, R. C., Sankalia, J. M., & Sutariya, V. B. (2007). Reversed chitosan–alginate
929 polyelectrolyte complex for stability improvement of alpha-amylase: optimization and
930 physicochemical characterization. *European journal of pharmaceutics and biopharmaceutics,*
931 *65*(2), 215-232.
932 Shao, P., Yu, J., Chen, H., & Gao, H. (2021). Development of microcapsule bioactive paper loaded with
933 cinnamon essential oil to improve the quality of edible fungi. *Food Packaging and Shelf Life, 27*,
934 100617.
935 Sittipummongkol, K., Chuysinuan, P., Techasakul, S., Pisitsak, P., & Pechyen, C. (2019). Core-shell
936 microcapsules of neem seed oil extract containing azadirachtin and biodegradable polymers and
937 their release characteristics. *Polymer Bulletin, 76*(8), 3803-3817.
938 Süfer, Ö., & Bozok, F. (2020). Characterization of essential oil from Matricaria sevanensis by microwave-
939 assisted distillation. *Journal of Thermal Analysis and Calorimetry, 140*(1), 253-261.
940 Sun, Z., Yang, C., Eggersdorfer, M., Cui, J., Li, Y., Hai, M., Chen, D., & Weitz, D. A. (2020). A general
941 strategy for one-step fabrication of biocompatible microcapsules with controlled active release.
942 *Chinese Chemical Letters, 31*(1), 249-252.
943 Tamayol, A., Akbari, M., Annabi, N., Paul, A., Khademhosseini, A., & Juncker, D. (2013). Fiber-based
944 tissue engineering: Progress, challenges, and opportunities. *Biotechnology Advances 31*(5), 669-
945 687.
946 Vandenberg, G., Drolet, C., Scott, S., & De la Noüe, J. (2001). Factors affecting protein release from
947 alginate–chitosan coacervate microcapsules during production and gastric/intestinal simulation.
948 *Journal of Controlled Release, 77*(3), 297-307.
949 Volić, M., Pajić-Lijaković, I., Djordjević, V., Knežević-Jugović, Z., Pećinar, I., Stevanović-Dajić, Z.,
950 Veljović, Đ., Hadnadjev, M., & Bugarski, B. (2018). Alginate/soy protein system for essential oil
951 encapsulation with intestinal delivery. *Carbohydrate Polymers 200*, 15-24.
952 Wang, W., Waterhouse, G. I., & Sun-Waterhouse, D. (2013). Co-extrusion encapsulation of canola oil
953 with alginate: Effect of quercetin addition to oil core and pectin addition to alginate shell on oil
954 stability. *Food Research International 54*(1), 837-851.
955 Wang, X., Zhu, J., Shao, T., Luo, X., & Zhang, L. (2019). Production of highly monodisperse millimeter-
956 sized double-emulsion droplets in a coaxial capillary device. *Chemical Engineering &*
957 *Technology, 42*(6), 1330-1340.
958 Yang, K., Liu, A., Hu, A., Li, J., Zen, Z., Liu, Y., Tang, S., & Li, C. (2021). Preparation and
959 characterization of cinnamon essential oil nanocapsules and comparison of volatile components
960 and antibacterial ability of cinnamon essential oil before and after encapsulation. *Food Control,*
961 *123*, 107783.

962 Zhang, L., Huang, J., Si, T., & Xu, R. X. (2012). Coaxial electrospray of microparticles and nanoparticles
963 for biomedical applications. *Expert Review of Medical Devices 9*(6), 595-612.

964

Figures:

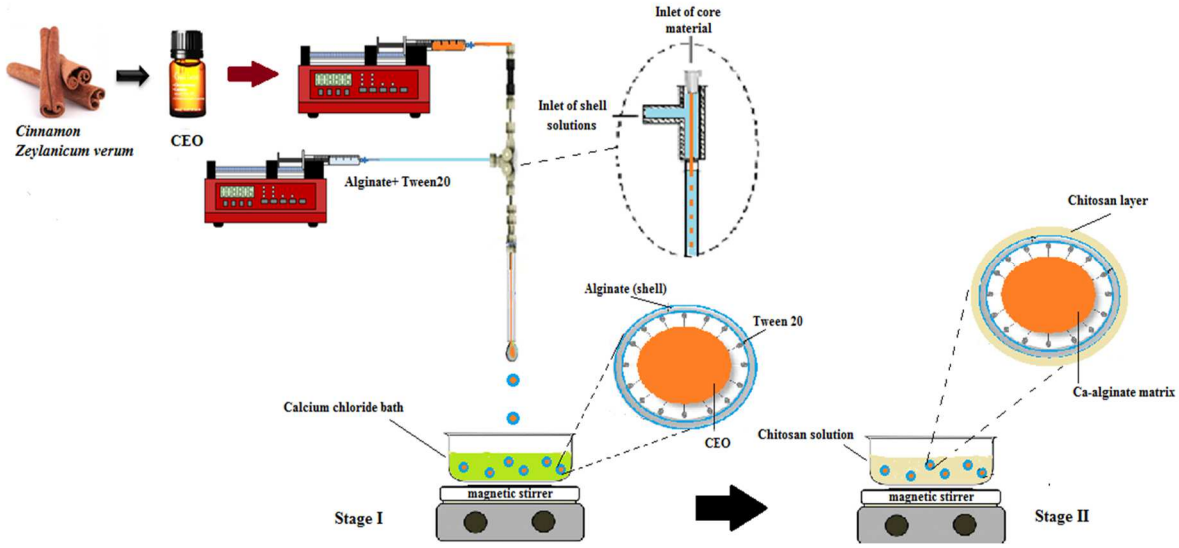

Fig. 1. Double-stage millifluidic method for preparing the oil-core millicapsules: CEO as dispersed phase is extruded through the co-axial flow into the alginate solution (continuous phase).

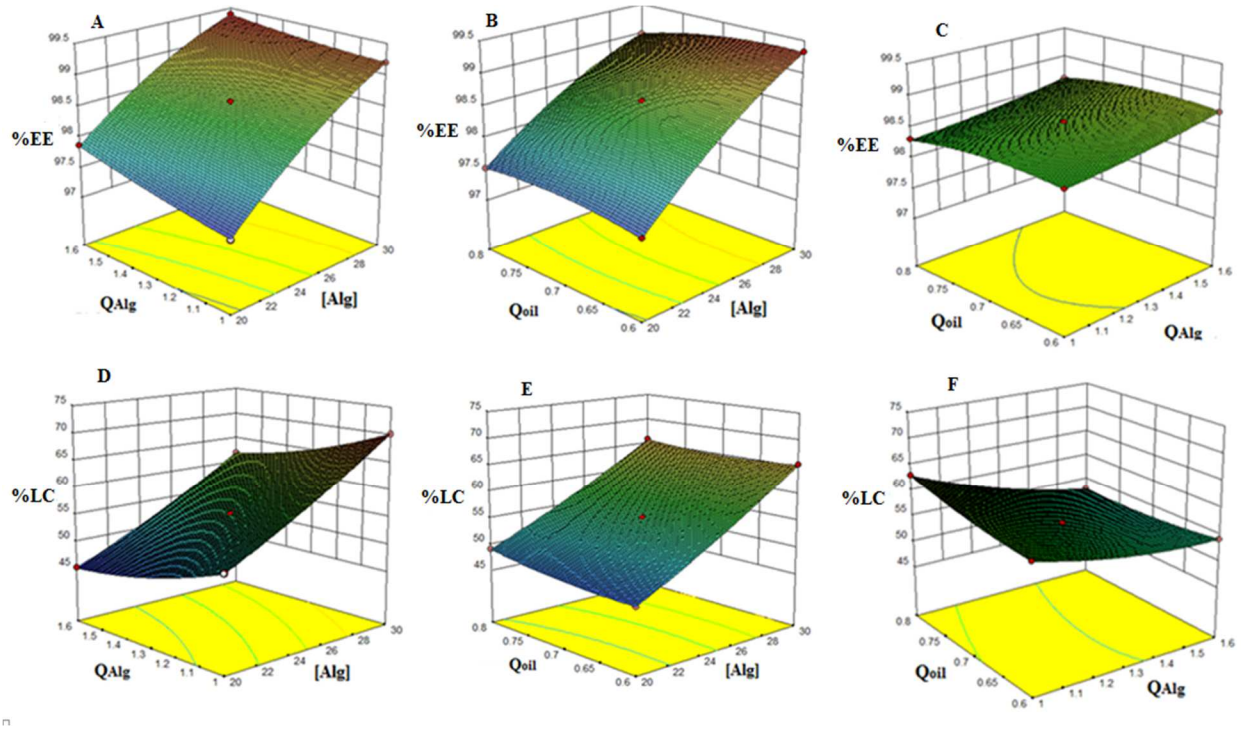

Fig. 2. Three-dimensional plots of the response surfaces for EE (**A-C**) and LC (**D-F**) as a function of concentration ([Alg]) and flow rate of alginate (Q_{Alg}) (**A, D**), alginate concentration ([Alg]) and flow rate of CEO (Q_{CEO}) (**B, E**), and flow rates of CEO (Q_{CEO}) and alginate (Q_{Alg}) (**C, F**).

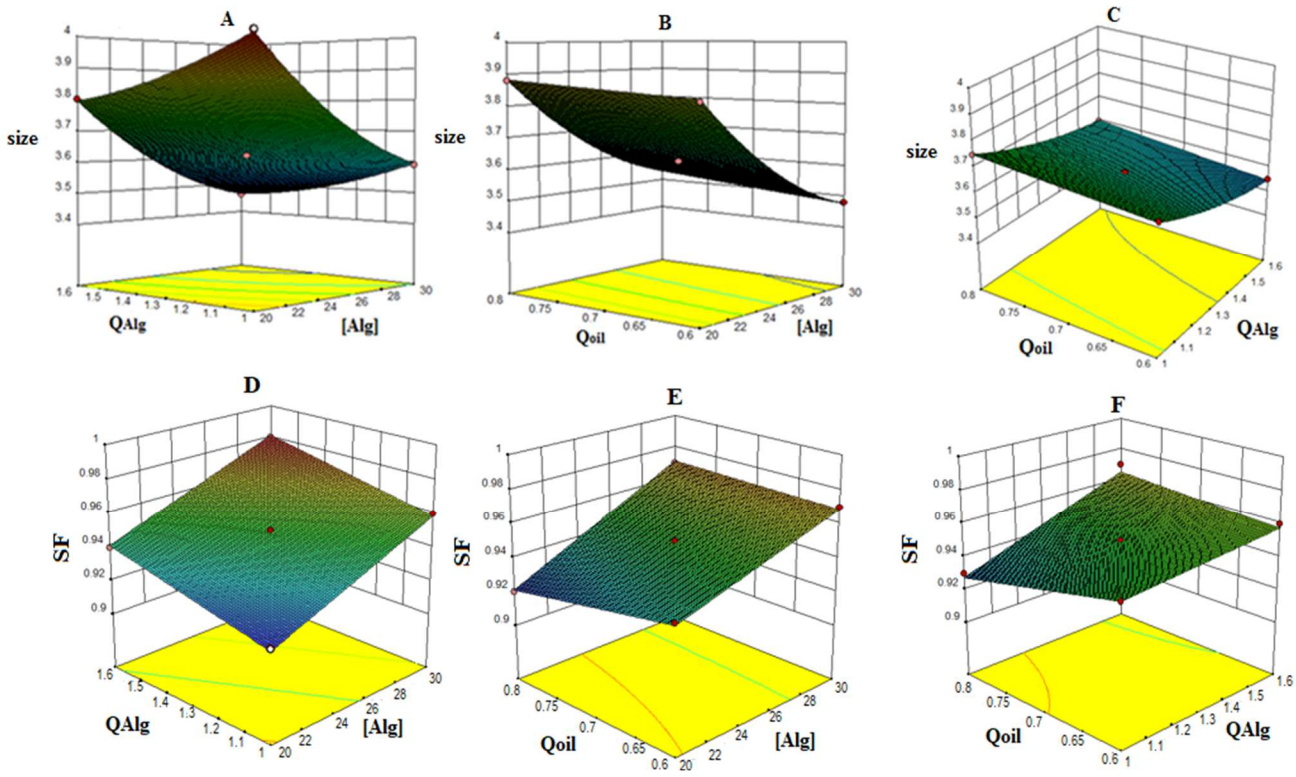

Fig. 3. Three-dimensional plots of the response surfaces for the size (A-C) and the SF (D-F) as a function of the concentration and the flow rate of alginate (A, D), the alginate concentration and the flow rate of CEO (B, E), and the flow rates of CEO and alginate (C, F).

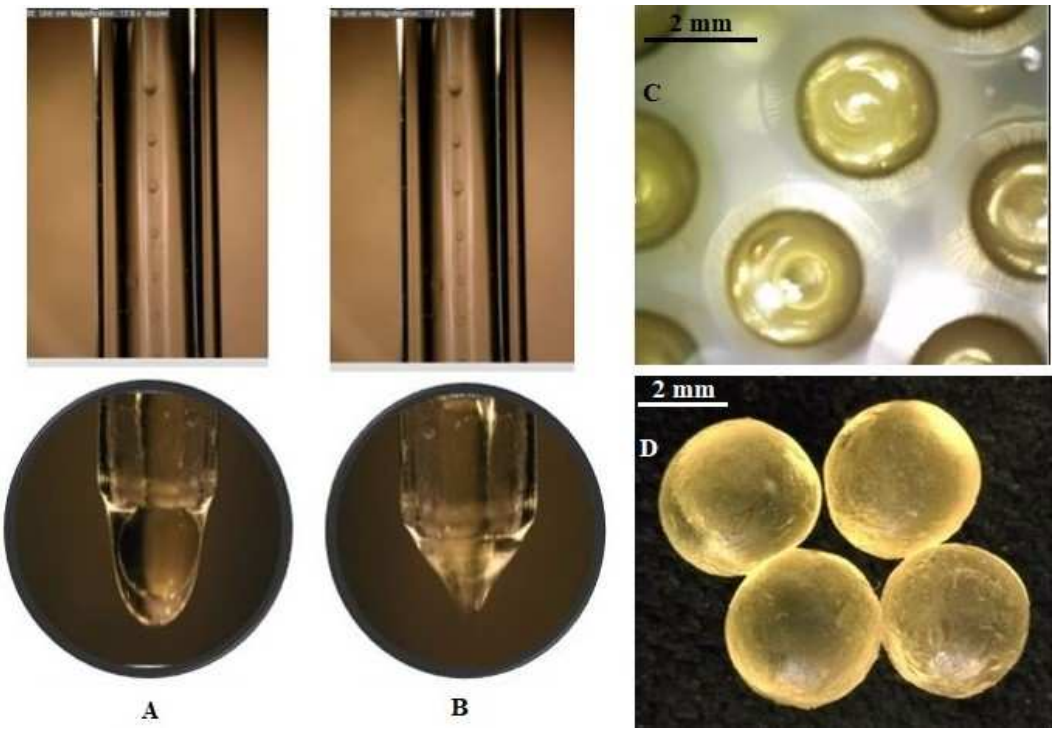

Fig. 4. Droplet formation pattern (A) and droplet detachment (B). Formation of optimal millicapsules at the moment of gelling (C) and after 30 min curing-time (D)

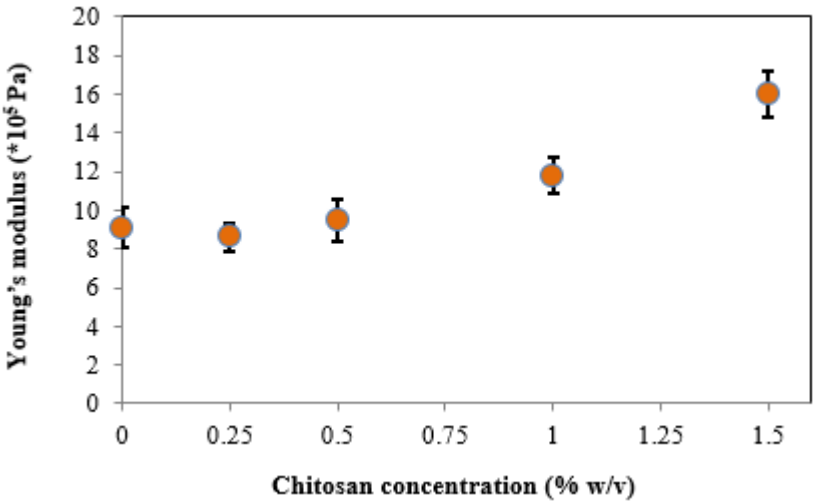

Fig. 5. Young modulus versus chitosan concentration for the optimal millicapsules

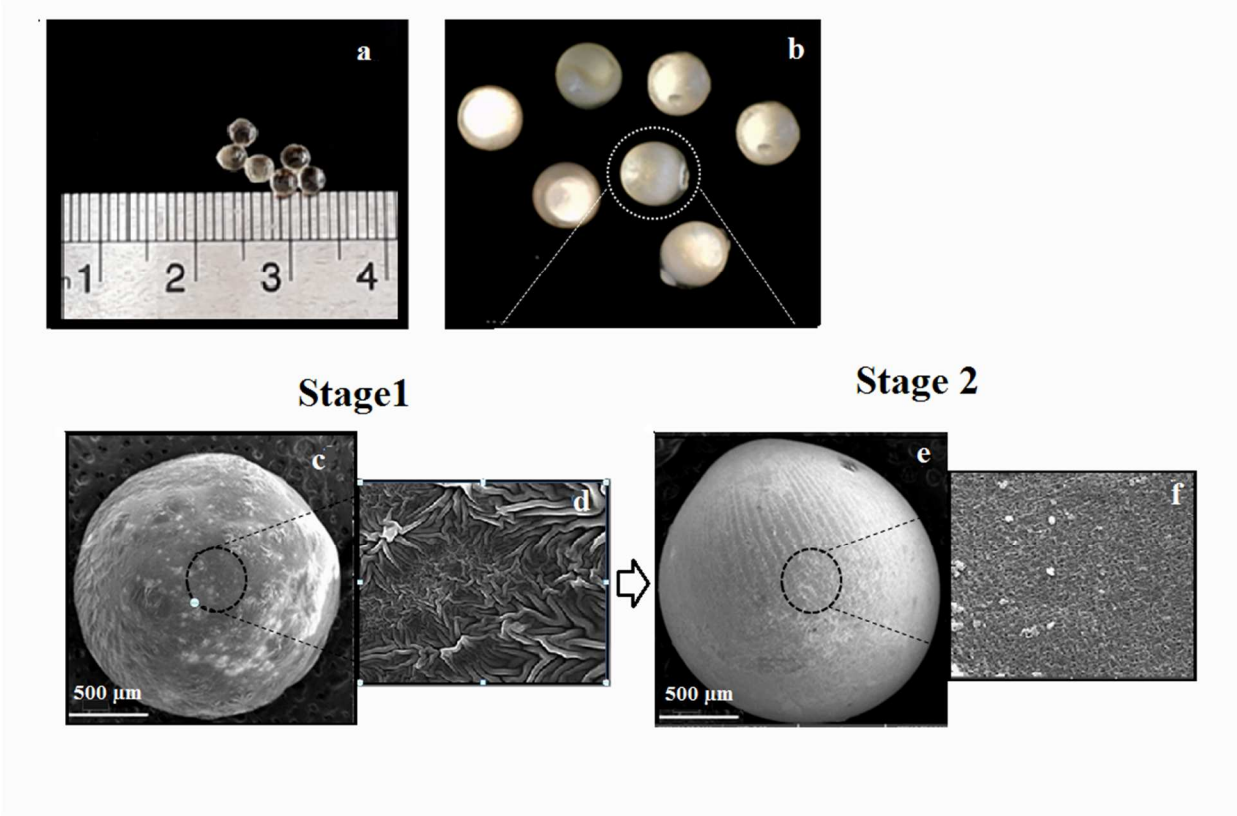

Fig. 6. Digital microscopy (a and b, ×30) and FESEM (c-f, ×80-500) images of CEO-loaded millicapsules (stage 1) and chitosan-coated millicapsules with CEO core (stage 2) prepared at the optimized conditions

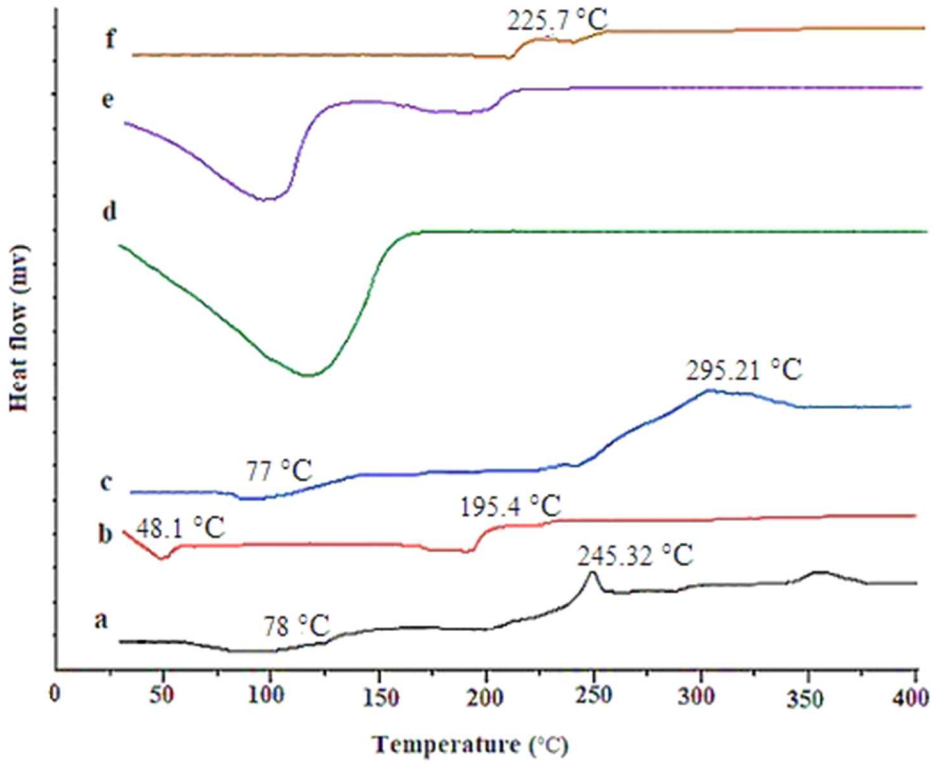

Fig. 7. DSC thermograms of sodium alginate (a), pure CEO (b), chitosan (c), unloaded millicapsule (d), CEO-loaded millicapsule (e), and chitosan-CEO- loaded millicapsule (f).

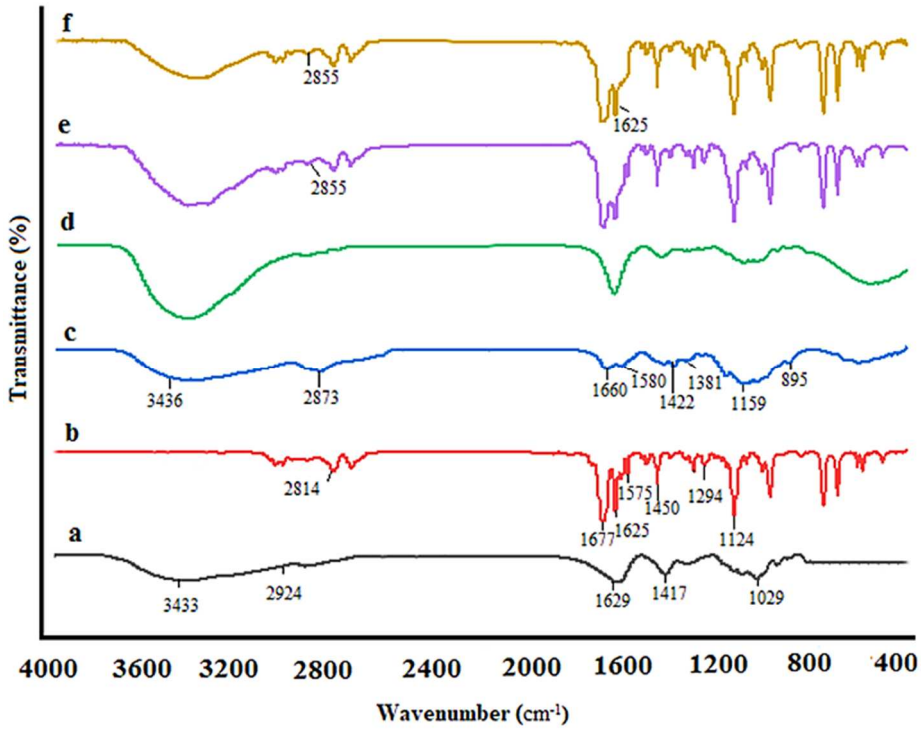

Fig. 8. FTIR spectra of sodium alginate (a), pure CEO (b), chitosan (c), unloaded millicapsules (d), CEO-loaded millicapsules (e), and chitosan-CEO- loaded millicapsules (f).

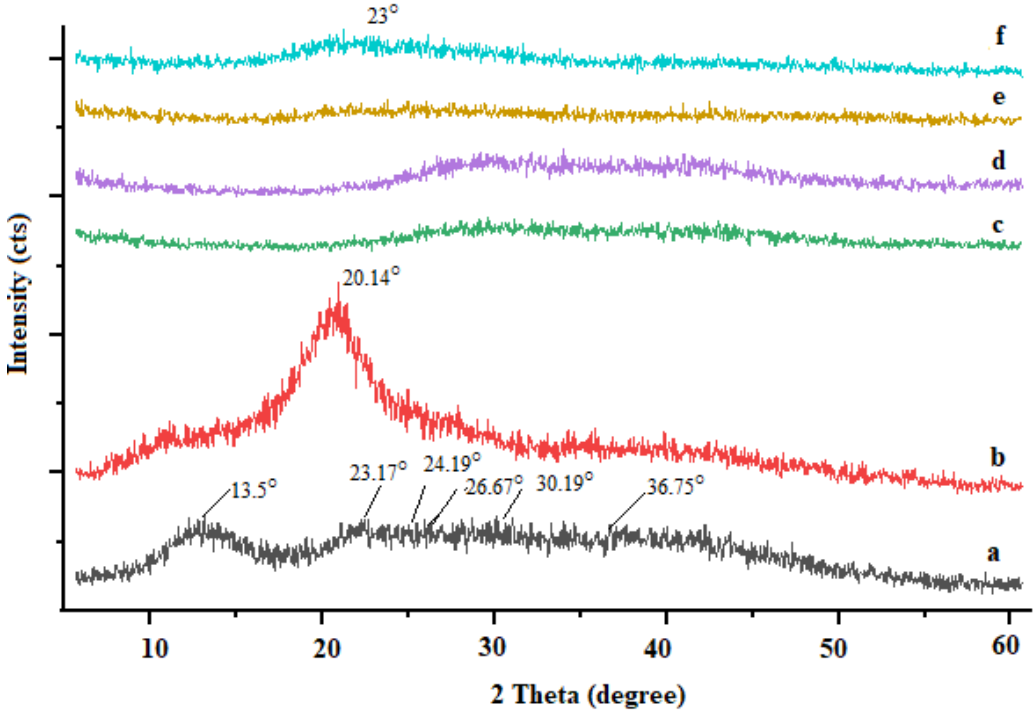

Fig. 9. XRD patterns of sodium alginate (a), chitosan (b), unloaded millicapsules (c), chitosan-unloaded millicapsules (d), CEO-loaded millicapsules (e), and chitosan-CEO- loaded millicapsules (f).

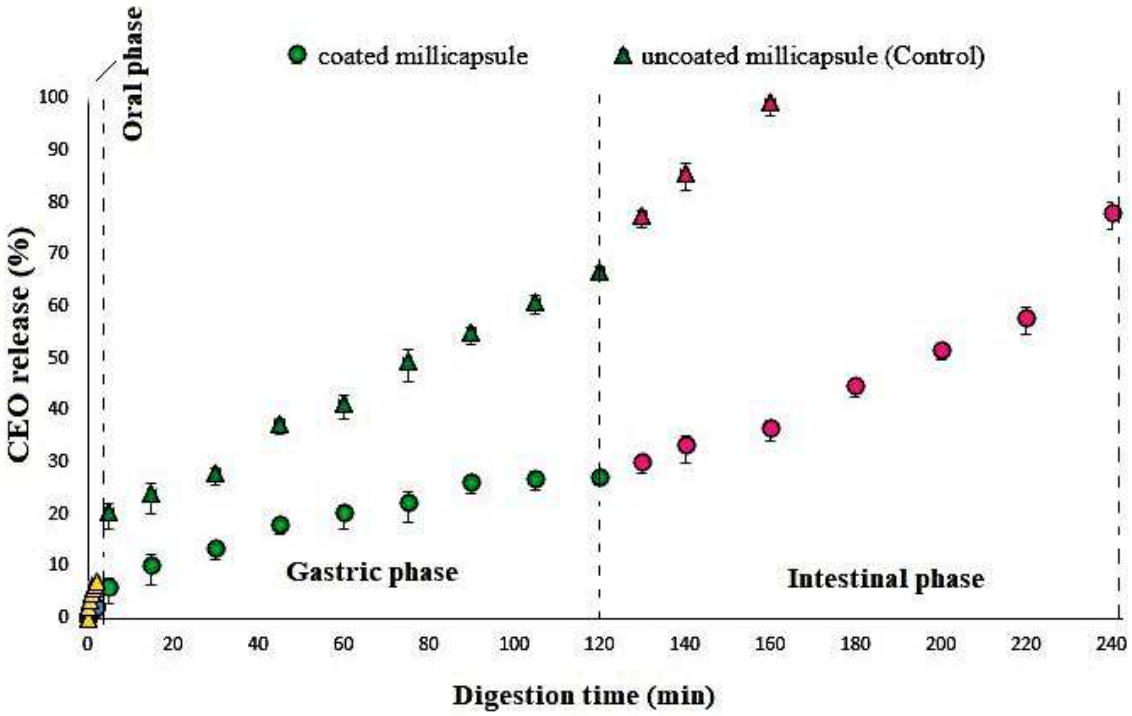

Fig. 10. The cumulative release profile of the cinnamon essential oil from the coated and uncoated millicapsules during in vitro digestion

Tables:

Table 1. Coded and uncoded factors for RSM ascertained from 17 experimental runs of Box-Behnken design

Run	Uncoded variables			Coded variables		
	[Alg], (g/L)	Q_{Alg}, (mL/min)	Q_{CEO}, (mL/min)	X_1	X_2	X_3
1	25	1.6	0.8	0	+1	+1
2	25	1.3	0.7	0	0	0
3	25	1.3	0.7	0	0	0
4	20	1.3	0.6	-1	0	-1
5	25	1.0	0.6	0	-1	-1
6	25	1.3	0.7	0	0	0
7	25	1.3	0.7	0	0	0
8	30	1.3	0.6	+1	0	-1
9	30	1.6	0.7	+1	+1	0
10	25	1.3	0.7	0	0	0
11	20	1.0	0.7	-1	-1	0
12	20	1.6	0.7	-1	+1	0
13	20	1.3	0.8	-1	0	+1
14	30	1.3	0.8	+1	0	+1
15	30	1.0	0.7	+1	-1	0
16	25	1.0	0.8	0	-1	+1
17	25	1.6	0.6	0	+1	-1

Table 2. Chemical compositions of the CEO identified by GC-MS

No	Compounds	Concentration (%)
1	Hexadecanol-2	0.70
2	Decane	6.27
3	M- Pyrol	3.38
4	Linalool	1.14
5	Cis-Cinnamaldehyde	0.58
6	Trans-Cinnamaldehyde	84.04
7	Eugenol	1.90
8	Alfa-Copaene	0.63
9	Caryophyllene	0.84
10	Cadina-1 (10),4-diene	0.49
11	Un-identified traces	0.03

Table 3. Second-ordered quadratic models developed for EE, LC, size and SF

Responses	Predicted models	R^2	R^2_{adj}	Covariance	Adequate precision
EE	Y_1 (EE) = 98.58+ 0.84 X_1+ 0.17 X_2- 0.05 X_3- 0.08 X_1X_2 – 0.10 X_1X_3 – 0.01 X_2X_3 – 0.16 X_1^2+ 0.03 X_2^2- 0.09 X_3^2	0.99	0.99	0.01	207.97
LC	Y_2 (LC) = 55.35+ 8.82 X_1- 3.77 X_2+ 0.65 X_3- 0.33 X_1X_2- 0.47 X_1X_3- 1.28 X_2X_3+ 0.73 X_1^2+ 1.21 X_2^2+ 0.71 X_3^2	0.99	0.99	0.1	568.80
Size	Y_3 (size) = 3.63- 0.18 X_1- 0.08 X_2+ 0.02 X_3+ 0.01 X_1X_2+ (5×10^{-3}) X_1X_3+ (5×10^{-3}) X_2X_3+ 0.05 X_1^2+ 0.02 X_2^2+ (10^{-3}) X_3^2	0.99	0.99	0.19	98.74
SF	Y_4 (SF) = 0.95+ 0.02 X_1+ 0.01 X_2- (3.75×10^{-3}) X_3+ (5×10^{-3}) X_1X_3+ (7.5×10^{-3}) X_2X_3	0.96	0.95	0.41	25.14

Table 4. Kinetics constant of cinnamon essential oil release profile in the simulated GIT (mouth, stomach, and small intestine)

Models	Parameters	Mouth		Stomach		Small intestine	
		coated	**uncoated**	**Coated**	**uncoated**	**coated**	**Uncoated**
Higuchi	K	0.03± 0.04	7.97± 0.11	2.61± 0.06	1.24± 0.09	0.51± 0.01	1.22± 0.19
	R^2	0.96	0.91	0.98	0.64	0.93	0.97
	RMSE	5.31	0.46	6.03	2.66	1.27	0.01
Ritger-Peppas	K	0.02± 0.01	4.64± 1.02	2.51± 0.17	5.86± 0.77	0.05± 0.01	0.25± 0.04
	n	1.02± 0.18	0.63± 0.03	0.51± 0.07	0.49± 0.31	1.33± 0.04	1.17± 0.08
	R^2	0.96	0.99	0.99	0.93	0.99	0.99
	RMSE	1.19	0.07	0.3	1.33	0. 7	0.08
Korsmeyer-Peppas	K	104.85±1.17	464.18± 2.43	272.35±3.44	58.61± 2.41	8.41±0.59	25.27± 1.76
	n	1.01±0.03	0.63± 0.03	0.49±0.01	0.49± 0.66	1.21±0.06	1.17± 0.06
	R^2	0.96	0.99	0.99	0.94	0.98	0.99
	RMSE	2.31	7.05	0.67	0.52	6.43	8.25
Kopcha	A	0.56± 0.04	3.44± 0.19	-0.22± 0.13	5.43± 0.72	-0.23± 0.3	-2.62± 0.55
	B	0.77± 0.02	1.17± 0.05	0.38± 0.06	0.04± 0.01	0.41± 0.02	0.83± 0.04
	R^2	0.95	0.99	0.82	0.96	0. 96	0.98
	RMSE	2.79	0.35	9.02	0.08	8.63	0.93

Cinnamon essential oil

Alginate+ Tween

Infuse

Infuse

Inlet of core material

Inlet of shell solution

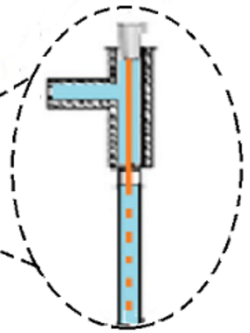

Alginate shell

Chitosan layer

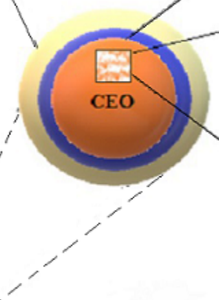

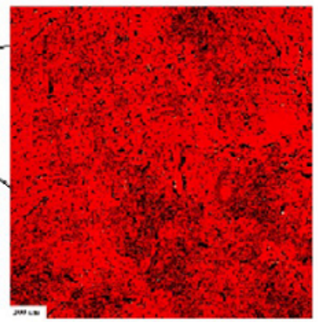

CLSM

Calcium chloride bath

magnetic stirrer

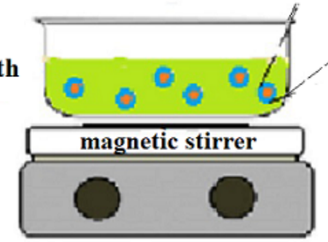

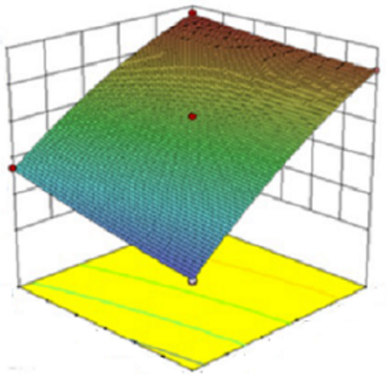

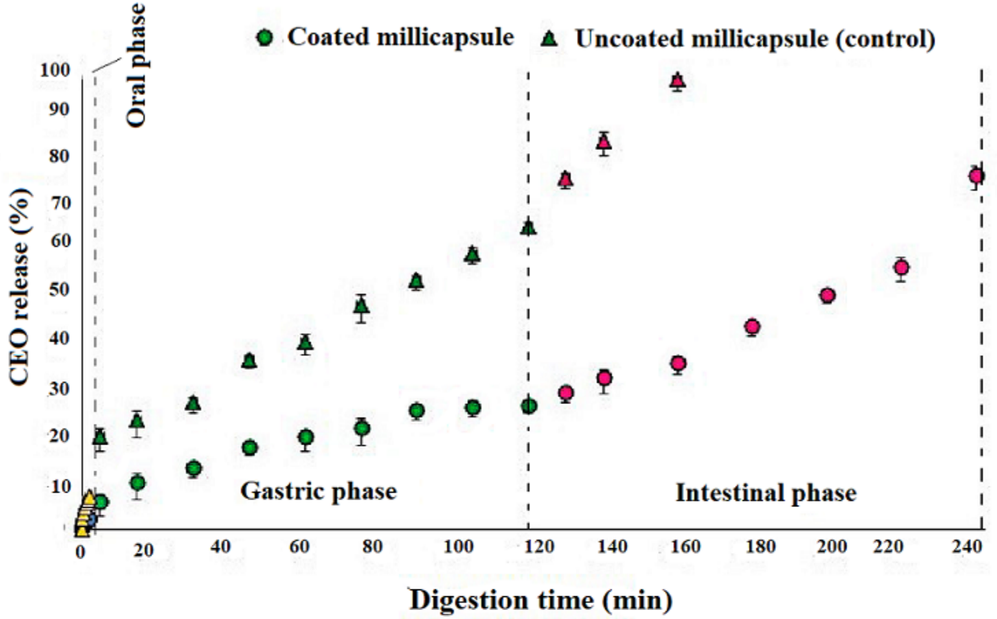

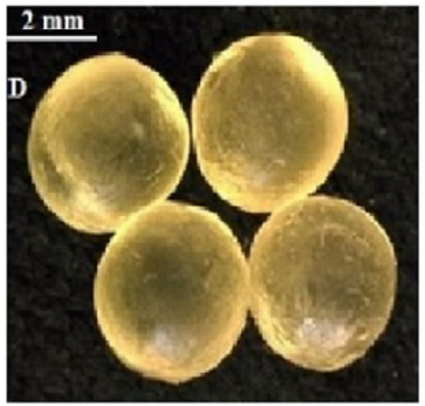

Optimal millicapsule